AIAA Journal
Vol. 50, No. 10, October 2012

Tailored Nozzles for Jet Plume Control and Noise Reduction

K. Viswanathan,* P. R. Spalart,† and M. J. Czech‡
The Boeing Company, Seattle, Washington 98124
A. Garbaruk§
New Technologies and Services, 197198, St. Petersburg, Russia
and
M. Shur¶
St. Petersburg State Polytechnic University, 195220, St. Petersburg, Russia

DOI: 10.2514/1.J051436

A synergistic utilization of computational simulations with experimental measurements is employed to develop dual-stream nozzle geometries that provide jet-noise reduction with the concurrent ability to control the orientation of the jet plumes, so as to minimize the thrust degradation associated with low-noise designs. The geometries consist of round primary and secondary nozzles, beveled primary nozzles, modified secondary nozzles, and combinations thereof. Specifically, the secondary nozzle is altered internally to provide the same deflection as a beveled primary in dual-stream exhaust geometry. The cross-sectional profiles are similar, but the bevel deflects the jet toward the short lip, whereas the modified secondary deflects the jet in the opposite direction. It is possible to eliminate/minimize the deflection of the total thrust vector through a judicious combination of the bevel and the modified secondary; numerical simulations facilitate this objective. The magnitude of the noise reduction increases with increasing primary jet velocity, and decreases with increasing flight Mach number. There is a gradual erosion of noise benefit as the azimuthal angle is increased from 0 deg (below the long lip of bevel). There is a benefit in effective perceived noise level for all the nozzle geometries evaluated in this investigation. The combinations of modified secondary nozzles with bevel 24 and bevel 30 provide the largest reduction in effective perceived noise level over a wide range of freestream Mach number, with a small thrust penalty. The design approach developed and evaluated here seems promising vis-à-vis practical applications, requiring only relatively limited modifications to an existing design. In addition, the modified secondary nozzle provides the ability to deflect the plume away from the underside of the wing and the flap, thereby reducing the jet-flap interaction noise.

I. Introduction

A joint computational and experimental program is carried out to assess the flow and noise characteristics of dual-stream nozzles. The geometries consist of round primary and secondary nozzles, beveled primary nozzles, modified secondary nozzles, and combinations thereof. The nozzles are designed in such a way as to allow maximum flexibility and interchangeability in the choice of primary and secondary nozzle combinations, so as to independently assess the effects of geometric variations on jet plume evolution and radiated noise. Ever since the introduction of the high bypass ratio (BPR) turbofan engine with dual-stream nozzles, there have been attempts to reduce the radiated noise through geometric variations to the nozzle exit shapes. The interest here is in nonaxisymmetric modifications on a larger scale. In addition to the establishment of the noise characteristics of dual-stream baseline circular nozzles since the 1970s (see [1–6] for a very brief list), there have been investigations of modified nozzles. One of the earlier studies is due to von Glahn and Goodykoontz [7], in which the primary and secondary nozzles were nonconcentric, with a thicker secondary jet in the flyover plane (toward the ground). Their results from a coplanar geometry indicated that there was 1) minor spectral changes at the lower radiation angles (measured from the inlet), and 2) a large reduction at the high-frequency portion of the spectra for radiation angles $\geq \sim 130$ deg. Bhat and Wright [8] illustrated various geometric arrangements in their 1981 patent and showed that the noise levels were lower in the azimuthal direction that corresponded to the thicker secondary shear layer.

The concept of providing a shielding low-speed layer for directional noise reduction has been revisited periodically ever since. Seiner and Krejsa [9] assessed the noise-reduction potential of several designs for noise reduction. A few nonconcentric nozzles were also evaluated in the 1990s as part of NASA's High Speed Civil Transport and Advanced Subsonic Technologies programs. More recently, Papamoschou [10,11] examined the acoustic and aerodynamic characteristics of flows from separate flow dual-stream nozzles, in which the shear layers were thickened in the downward and sideline directions through the use of wedges, pairs of vanes, or flaps in the secondary flow. All these mechanisms for flow modifications were based on the principle of setting up a thicker shielding layer; another interpretation is that the merging of the inner and outer shear layers, and the associated surge in turbulence are delayed and made more benign. Good noise reduction was observed with all these geometric additions; noise benefits in the effective perceived noise level (EPNL, EPNdB) of 2.1 EPNdB in the downward direction and 1.0 EPNdB in the sideline directions were reported. Zaman and Papamoschou [12] and Zaman et al. [13] tested the same concepts at the NASA John H. Glenn Research Center at Lewis Field; the geometries were identical to those in [10,11], but eight times larger. They found some noise benefit for jets with low to moderate BPRs. However, the magnitude of noise benefit was found to be substantially lower for the bigger scale nozzle at the NASA John

Presented as Paper 2011-2788 at the 17th AIAA/CEAS Aeroacoustics Conference , Portland, OR, 6–8 June 2011; received 12 June 2011; revision received 1 February 2012; accepted for publication 4 February 2012.

*Technical Fellow, Aeroacoustics and Fluid Mechanics; k.viswanathan@boeing.com. Associate Fellow AIAA.
†Senior Technical Fellow, Aeroacoustics and Fluid Mechanics; philippe.r.spalart@boeing.com. Member AIAA.
‡Aeroacoustics Engineer; michael.j.czech@boeing.com. Member AIAA.
§Associate Professor; agarbaruk@cfd.spbstu.ru.
¶Leading Research Scientist; mshur@cfd.spbstu.ru. Senior Member AIAA.

H. Glenn Research Center at Lewis Field. All of these studies were restricted to static jets.

Majjigi et al. [14] first evaluated the shielding idea in a free jet facility, with forward flight. They discovered that the large reduction observed for the static case is almost completely absent in the peak noise radiation sector when a flight stream is introduced. Bridges and Henderson [15] and Brown et al. [16] assessed the concepts of vanes and wedges, along with the shaping of the fan flow (called S-duct in their terminology) at the NASA John H. Glenn Research Center at Lewis Field, and provided a comprehensive evaluation of offset-stream technologies. The design of the secondary nozzle to adjust the offset streams in this study has similarities with the S-duct. The notable aspect of this NASA program is a realistic evaluation with a forward flight stream. Furthermore, the offset-stream concepts were examined at three BPRs of 5.0, 8.0, and 13.0, with measurements of flow and noise. Acoustic data were acquired both at static condition and with a tunnel Mach number (M_t) of 0.2. Cross-sectional profiles of the flow confirmed the as-intended thickening shielding layer in the downward direction. A noise benefit at static conditions was observed at the lower BPRs. However, there was substantial increase of the spectral level at the higher frequencies, especially over a wide range of lower polar angles with forward flight. In the important metric of EPNL, the noise benefit completely disappeared with the addition of a flight stream for all the concepts and at all the BPRs. Figure 1, reproduced here from the NASA John H. Glenn Research Center at Lewis Field test, summarizes the main findings. This test program produced definitive trends and represents the status of the offset-stream technologies. In addition, the importance of evaluating any noise-reduction concept under realistic conditions is highlighted once again. This state of affairs brings the authors to the current study, which is described in the following section.

II. Scope of Current Study

The previously mentioned ideas for shielding rely on modifying the fan or secondary stream to produce a thicker fan layer in the desired azimuthal directions. Viswanathan [17–19] recently reported on the noise benefits that can be obtained with beveling the primary nozzle. Good noise reductions were observed for both single-stream and dual-stream nozzles; for dual-stream nozzles, the secondary nozzle was unaltered. Substantial noise reduction in the peak noise radiation sector was demonstrated for both single and dual jets, in the angular range $\geq \sim 120$ deg. Further, there was no noise increase at the higher frequencies, in contrast with chevron nozzles. Noise benefit in EPNL, although lower with forward flight, was realized even with a flight Mach number of 0.32. See figure 17 in [18]. There is a key difference between the beveled nozzle and the shielding

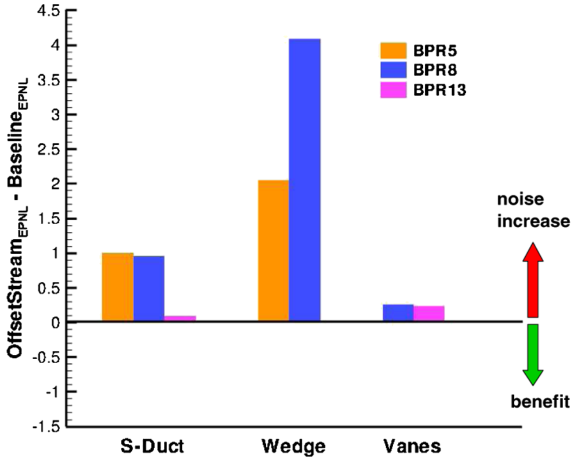

Fig. 1 Effect of offset stream concepts on EPNL at typical takeoff power and various BPRs. $M_t = 0.20$. (Reproduced from [16].)

concepts, as discussed by Viswanathan [18] in Sec. IV.B (p. 624). It is important to realize that for a single jet, there is no thickening layer (or any layer for that matter) surrounding the jet. Yet, dramatic reductions in noise have been measured below the longer lip of the beveled nozzle. Therefore, the physics of noise reduction is very different for the beveled nozzle and is not connected in any way to the shielding concepts that have been attempted in the last 30 years.

A detailed Reynolds-averaged Navier–Stokes (RANS) and large eddy simulation (LES) computational study of single-stream and dual-stream beveled nozzles, along with those of round nozzles, was carried out to gain better insights into the flow features responsible for noise reduction; see Viswanathan et al. [20] for complete details. Two sample flowfield results from [20] illustrate the differences in the jet evolutions. Figure 2 shows the instantaneous vorticity fields in the symmetry plane of the LES for the three nozzle geometries; the secondary nozzle is round for all three cases and the primary nozzle consists of a round nozzle, and two bevels with bevel angles (measured from the vertical nozzle exit plane for the round nozzle) of 24 and 45 deg, respectively. Aside from the plume vectoring, there is significant alteration of the turbulence structure of the jets. The fan streams of the beveled nozzles are highly asymmetric with the top being narrower and the bottom substantially thicker than those for the round jets, after the top one begins merging with the core shear layer; this effect is much stronger for the bevel 45 system. The fan flow needs to accommodate the upward deflection of the core stream, which stretches it on the upper side, resulting in the thinning of the shear layer; conversely, there is lateral streamline convergence and thickening on the lower side. The modifications to the potential-core lengths are also highlighted by the vorticity fields: 1) as for the single jets, the length of the primary potential core is reduced as the bevel angle is increased; 2) the length of the secondary shear layer at the top is progressively shortened with increasing bevel angle; and 3) the behavior of the bottom shear layer is different for the two beveled nozzles; it is somewhat longer than the round for bevel 24, and shorter than the round for bevel 45 due to the rapid widening of the outer shear layer. The secondary potential core is defined as the flow area between the two streams, free of vortical structures.

Several interesting features are observed when the cross-sectional contours of vorticity from the RANS computations at several axial stations are examined for the static case in Fig. 3. For the conventional nozzle, there are, of course, concentric rings of vorticity, mainly concentrated in the shear layers in the early mixing layers. As the flow evolves, these get gradually mixed out, but retain their axisymmetric shape at all downstream locations. For the beveled nozzles, the region of high vorticity migrates toward the shorter side of the beveled nozzle, and the plume gets elongated in the vertical plane. The fan flow (mixed with the ambient air) gets pulled toward the center of the core jet, and the primary shear layer takes on a C shape. The secondary shear layer is highly asymmetric, much thicker at the bottom, as also seen in the plots of instantaneous vorticity from the LES in Fig. 2. Additional information may be found in [20].

The interesting flow features displayed in Figs. 2 and 3 contrast the different evolutions of the jet plumes. Now, one could produce nearly the same flow cross-sectional patterns without beveling the primary nozzle, but through suitable shaping of the secondary nozzle. It is important to keep in mind that the precise mechanisms responsible for the generation and radiation of sound from high-Reynolds-number turbulent flows are not completely known, and the causal connection between flow/turbulence and noise generation has yet to be established quantitatively. This point is discussed in greater length in [20]. However, the approach taken here is to design a dual-stream nozzle system with a round primary nozzle that mimics the flow features observed in Figs. 2 and 3. Two such secondary nozzles, hereafter referred to as modified fan nozzles MF1 and MF2, have been designed using the computational procedure. MF1 produces a weaker effect and MF2 produces a stronger effect. In the initial study of beveled nozzles by Viswanathan [17–19], no attempt was made to control the plume deflection; rather, the deflection angles for the various geometries and cycle conditions were established from the

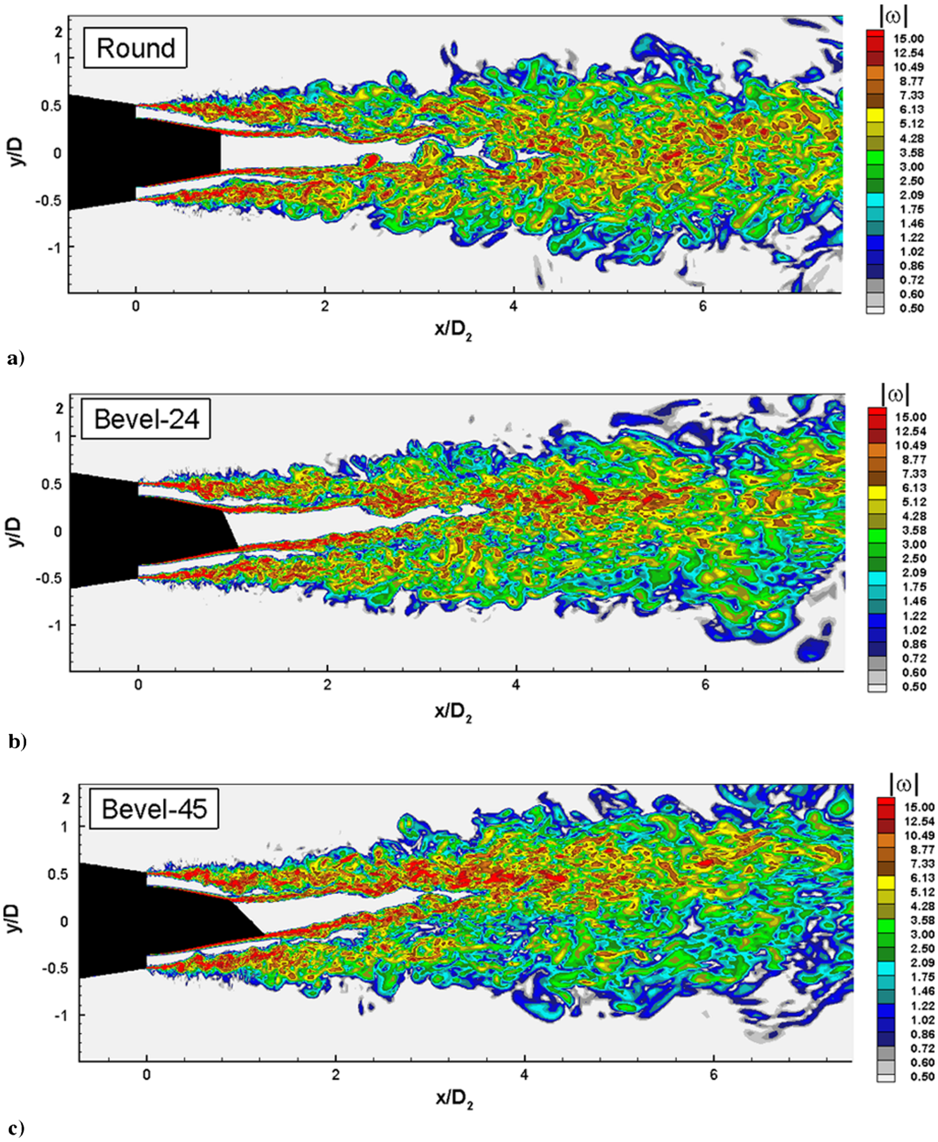

Fig. 2 Effect of primary-nozzle beveling on snapshots of vorticity for a dual-stream jet. $NPR_p = NPR_s = 1.8$, $T_p/T_a = 2.37$, $T_s/T_a = 1.0$. a) round, b) bevel 24, and c) bevel 45.

force measurements obtained with a six-component force balance. As seen in Figs. 2 and 3, the plume deflects toward the short lip of the beveled nozzle for convergent beveled nozzles at all nozzle pressure ratios (NPRs). One could tailor the secondary nozzles MF1 and MF2 in such a way as to counteract the plume deflection caused by a beveled primary nozzle and precisely align the total thrust axis. Regardless of the noise-reduction potential of a modified secondary nozzle, now there is a way to control the jet plume with any given beveled primary nozzle. This would make the application to an existing design less disruptive; the deflection of the fan stream could also weaken jet-flap interaction.

A detailed aeroacoustic wind-tunnel test has been carried out to address the following questions: 1) would a modified secondary nozzle yield noise reduction by itself? 2) if so, would the noise benefit together with a beveled primary nozzle be additive? 3) can the thrust alignment be controlled with this design approach? 4) does the noise reduction correlate well with flow features in steady computational fluid dynamics (CFD) solutions (as opposed to LES), such as the relative positions of shear layers? This fourth point would be most helpful in industrial practice, for installed engines. From a practical standpoint, it was decided to create a wider database with four different primary beveled nozzles with bevel angles of 18, 24, 30, and 36 deg, and two modified secondary nozzles. MF1 produces a weaker deflection and MF2 a stronger deflection in a direction opposite to those of the beveled nozzles. An equivalent round nozzle system was employed to generate baseline data for comparison. Aeroacoustic data have been generated with all possible combinations of baseline and modified nozzles. Results from the experimental study, together with computed flowfields, are presented in this paper.

III. Overview of Computational Procedure

The numerical system developed by Shur et al. [21–23] is used for the investigation of the aeroacoustics of the nozzles considered. Therefore, only a brief overview of the prediction procedure is needed here. A high-order computer code, described by Strelets [24], is run on structured multiblock curvilinear grids. The versatility and the robustness of the code were demonstrated for a variety of aerodynamic flows, and excellent comparisons with benchmark experimental data were shown in [24]. For jet-noise predictions, the turbulence is treated by LES and the far-field noise is computed with the Ffowcs Williams–Hawkings [25] formulation. The Navier–Stokes equations are solved with a slightly upwind-biased high-order differencing for spatial discretization and implicit time integration. The time integration is carried out with a second-order three-layer

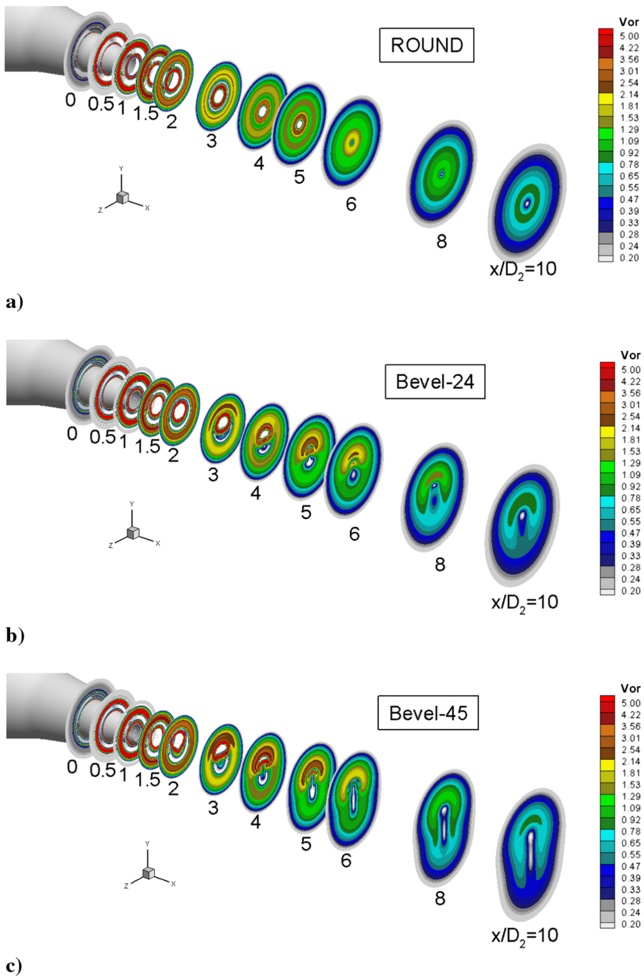

Fig. 3 Vorticity contours for the dual-stream jets at various cross sections. $NPR_p = NPR_s = 1.8$, $T_p/T_a = 2.37$, $T_s/T_a = 1.0$. a) round, b) bevel 24, and c) bevel 45.

backward scheme and dual time stepping. In the turbulent-flow region and in the near field, the spatial discretization uses a combination of fourth-order centered and fifth-order upwind-biased scheme based on flux-difference splitting for the inviscid terms. Outside this region, purely upwind differencing is employed to damp out the outgoing waves. A buffer layer, in addition to nonreflecting boundary conditions, is included to ensure that reflections from the boundaries do not contaminate the solution in the domain of interest. For simulating the turbulence, the subgrid-scale model is deactivated and the approach is viewed as implicit LES. The slight dissipation introduced by the upwind scheme (with a typical weight of 0.25) serves the purpose of removing the energy that would be transferred to the unresolved scales as part of the energy cascade. Several other approaches were evaluated as well; this choice turned out to be the best option for simulating realistic transition to turbulence, as explained in [21–23]. First, large eddy simulations for the flow and noise were carried out for the baseline and modified nozzles to assess the noise-reduction potential. Based on the LES results, the contours of the nozzles were refined until promising geometries were identified. Two preferred secondary geometries (MF1 and MF2), along with four beveled primary nozzles, were finally fabricated for wind-tunnel testing. Noise predictions using LES for the different geometries are not included here. Instead, computed flowfields using RANS and extensive experimental results are presented.

The computations are performed with the use of the ν_t-92 model, which is a one-equation linear isotropic eddy-viscosity transport model developed since the 1970s by Secundov [26,27], and is more attractive than other common models for round jets because of a correction term activated by the curvature of the eddy-viscosity contours (however, this becomes active in the fully developed jet region, not in the thin mixing layers that separate the potential cores). It also contains a compressibility correction, which is felt in sonic mixing layers. The complexity in the present flows is primarily inviscid in nature: transverse pressure gradients and compressibility on the potential core. The boundary layers remain thin and attached, thanks to the contraction so that the impact of turbulence-modeling imperfections is slight.

For RANS simulations, the computations are performed on a two-block grid with a total of about 2.5 million cells. The grid topology is described in detail in [20,21]. The central Cartesian block has $261 \times 18 \times 18$ cells in the axial and lateral directions, whereas the outer cylindrical block has $311 \times 106 \times 72$ cells in the axial, radial, and azimuthal directions, respectively. The grid has been shown to provide virtually grid-independent solutions. The grid used in LES has similar topology, but the total number of grid points is ~ 5 million: $321 \times 18 \times 18$ in the inner block and $493 \times 135 \times 72$ in the outer block. As shown in [20], this grid ensures agreement of the predicted and experimental far-field noise spectra with an error not higher than 3 dB within the frequency range up to 15 kHz ($St = \sim 5$, based on the fan diameter and core jet velocity). In this paper, the mean flow profiles and contours from only the RANS simulations are presented.

IV. Experimental Program

The aeroacoustic test has been carried out at The Boeing Company's Low Speed Aero Acoustic Facility. Detailed descriptions of the test facility, the jet simulator, the data acquisition and reduction process, etc. may be found in [28,29]. For the sake of completeness, a brief overview is provided here. Brüel & Kjær quarter-inch type 4939 microphones are used for free-field measurements. The microphones are set at normal incidence and without the protective grid, which yields a flat frequency response up to 100 kHz. Typically, several microphone arrays are used; these arrays are at a constant sideline distance of 15 ft (4.572 m) from the jet axis and on a polar arc of 25 ft (7.62 m). All angles are measured from the jet inlet axis and cover a polar range of 50–150 deg. Very fine narrow band data with a bin spacing of 23.4 Hz up to a maximum frequency of 88,320 Hz are acquired and synthesized to produce one-third octave spectra, with a center band frequency range of 200–80,000 Hz. The jet simulator is embedded in a free-jet wind tunnel, which can reach a maximum Mach number of 0.32. The dimension of the wind tunnel is 9×7 ft. The jet simulator is incorporated with a six-component force balance, and simultaneous measurements of thrust and noise are acquired.

The diameter of the baseline primary nozzle is 2.08 in., and the area ratio between the secondary and primary nozzles (A_s/A_p) is 3.92. The subscripts p and s denote primary and secondary, respectively. Recall that convergent beveled nozzles were tested in Viswanathan [17] and are also used here. From the experimentally measured actual mass flow rate for given plenum conditions with a critical flow venturi, it was established in [17] that the effective flow area for the beveled nozzles is lower than the geometric area (in the slant plane). This reduction in flow area is attributable to nonuniform pressure distribution at the exit plane and has been confirmed with numerical simulations in [20]. The center plug in the dual-stream nozzle geometry tested could be moved in the axial direction, thereby providing ability to control and set the annulus flow area. In the current test program, RANS simulations for the four beveled nozzles were first carried out, and the computed mass flow rates for the four beveled nozzles were compared with the corresponding mass flow for a round nozzle, for fixed plenum conditions. Based on the reduction, the exit area for each beveled nozzle was increased by suitably setting the annulus flow area such that the mass flow rate matched that of the round nozzle. It was also verified through RANS simulations that the mass flow rates for the modified fan nozzles matched the mass flow rate for the baseline round secondary nozzle; the discrepancies in mass flow rates were $\leq 0.3\%$ for all geometries. In strict terms, the secondary flow path is altered in the desired fashion without modifying the exit area, using slight S shaping upstream. Thus, the nozzle exit areas were chosen to produce the same mass flow rates for all the nozzles.

V. Computed Flowfields

Sample flow computations using RANS are presented to highlight the changes to the flowfield due to modifications of the nozzle geometries, and emphasize the approach for controlling the jet plume and presumably reducing its noise. An extensive set of nozzle geometries, both primary and secondary, was considered and analyzed with RANS computations before the decision to fabricate the four beveled primary nozzles and two modified secondary nozzles. First, the possibility to produce the same flow features observed for the primary beveled nozzles (with round secondary) through suitable tailoring of the secondary nozzle alone (with round primary) is demonstrated. Figure 4 shows side-by-side comparisons of contours of streamwise velocity in the cross-sectional planes; six different axial stations are considered. The jet operating conditions are as follows in all the computational results shown: $NPR_p = NPR_s = 1.8, T_p/T_a = 2.37, T_s/T_a = 1.0$, and $M_t = 0.20$. The velocity contours for the baseline (round + round) are on the left-hand side and the modified nozzles on the right. In Fig. 4, contours are presented for the baseline and bevel24 + round. The axial distance is normalized by the diameter of the secondary jet (D_2). The evolution and spreading of the jet with downstream distance, with progressively larger cross-sectional areas, are evident. Whereas the jet shape is concentric for the baseline, the increasing distortion and stretching of the jet in the vertical plane produce an oval shape for the bevel 24 primary nozzle. The deflection of the jet toward the short lip of the beveled nozzles (toward the top in the figure) is also obvious; the trends are similar to those seen in Fig. 3. Figure 5 shows a comparable flowfield obtained through the modification of the secondary nozzle alone. Note that the flow is deflected downward, but the gross features are similar to those seen in Fig. 4. For instance, the plume shape is oval, with stretching in the vertical plane and progressive distortion with increasing downstream distance. Closer attention to the contours in Figs. 4 and 5 at $x/D_2 = 6$ reveals that the contour shapes of different velocities and corresponding areas are similar.

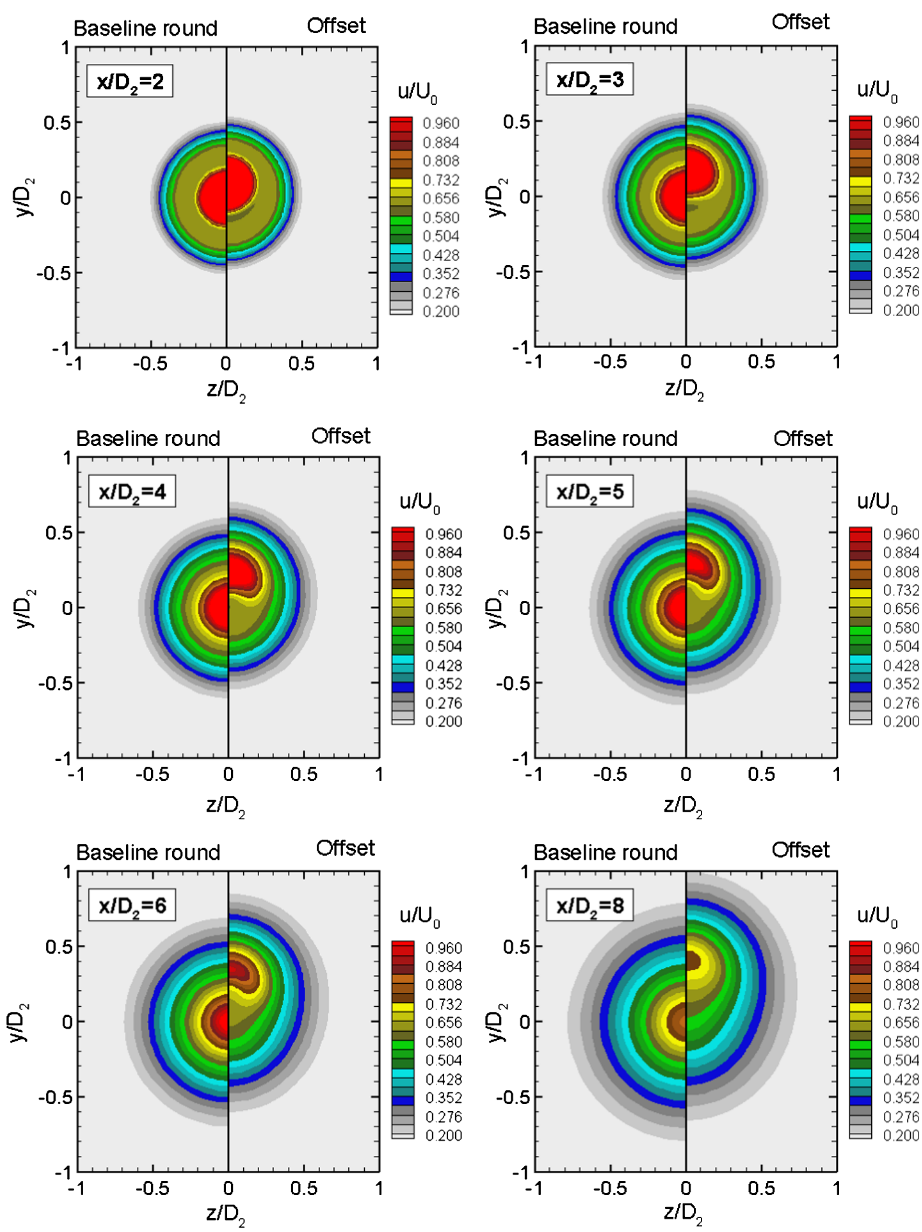

Fig. 4 Streamwise velocity in cross-sectional plane. $NPR_p = NPR_s = 1.8$, $T_p/T_a = 2.37$, $T_s/T_a = 1.0$, and $M_t = 0.20$. Left: baseline (round + round); right: bevel24 + round.

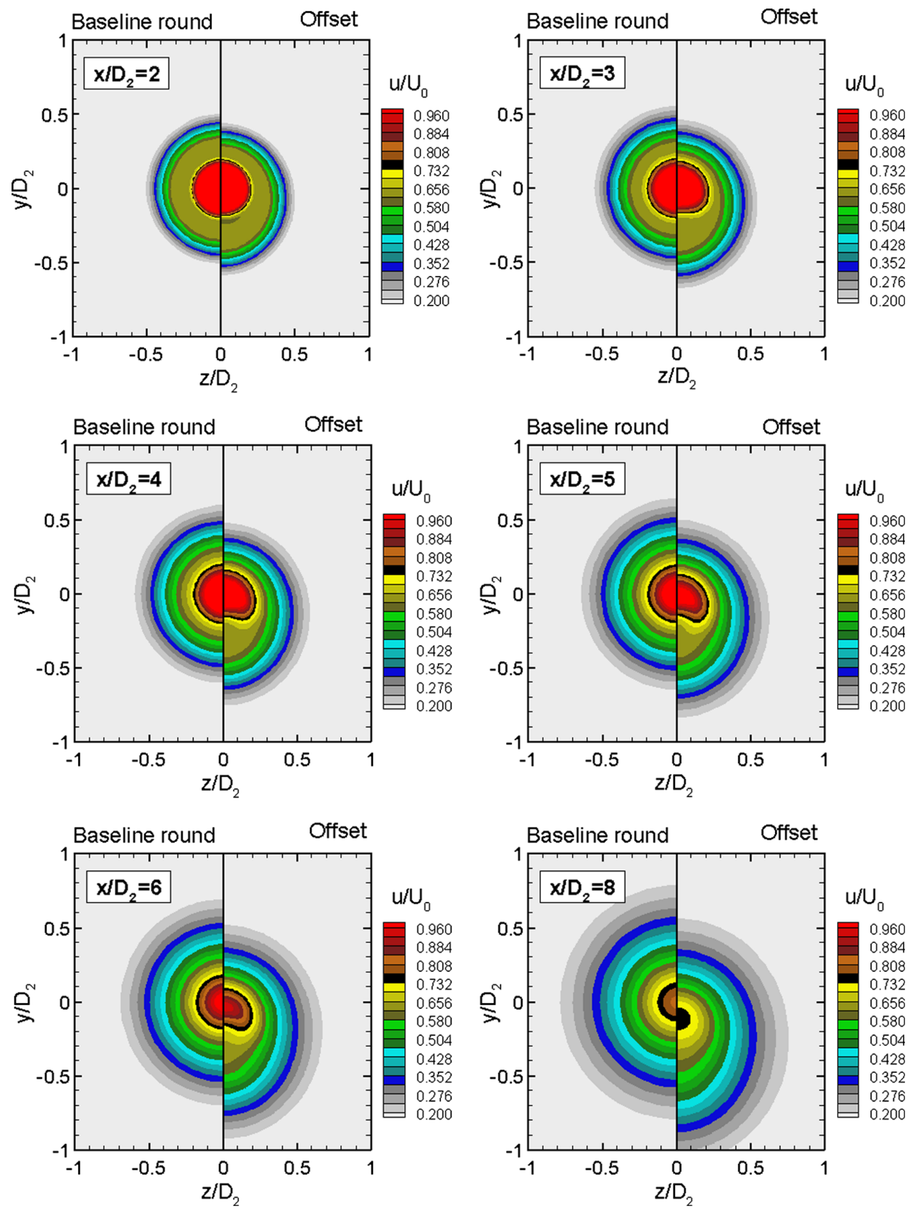

Fig. 5 Streamwise velocity in cross-sectional plane. $NPR_p = NPR_s = 1.8$, $T_p/T_a = 2.37$, $T_s/T_a = 1.0$, and $M_t = 0.20$. Left: baseline (round + round); right: round + modified A.

Next, a larger bevel angle of 45 deg and a correspondingly larger deflection of the plume in Fig. 6 are considered. As expected, the effects of this larger bevel angle are more pronounced than those of bevel 24. An equivalent flowfield obtained through the modification of the secondary nozzle is shown in Fig. 7; the degree of nozzle modification is larger to closely duplicate the larger effect due to bevel 45. Again, the flow features are comparable. It is clear that the design procedure adopted for modifying the secondary nozzle alone produces similar flow features obtained through the beveling of the primary nozzle and a round secondary nozzle. It should be noticed though that the plume deflection is in the opposite direction.

Sample computed flows with combinations of different beveled primary nozzles and modified secondary nozzles are now presented to illustrate the ability to control the plume vectoring. An examination of the variation of axial velocity in the symmetry plane of the jet, with downstream distance, highlights the various effects. Such a variation is depicted in Fig. 8 for the baseline, bevel 45, strongly modified secondary, and a combination of bevel24 + modified secondary nozzles. These axial contours indicate that the bevel deflects the plume upward, the modified secondary deflects the plume downward, and the combination more or less aligns the jet plume with the x axis. The reduction in potential-core lengths for all the modified nozzles, when compared with the baseline nozzle, is also evident. A comparison of the baseline and (bevel24 + modified secondary) highlights the stark differences in the flowfields between the two geometries, although the plumes are aligned with the x axis.

The degree of modification to the secondary nozzle is controlled by a geometric parameter; the higher the value of this parameter, the larger the plume deflection. The criterion for plume alignment with the x axis is the following: find a suitable value for this parameter that would reduce the vertical force to zero or within a small tolerance. This exercise was carried out for three bevel angles of 15, 20, and 24 deg. The computed normal forces were $\leq 0.08\%$ for all cases. The resulting computed flowfields in the cross-sectional planes are shown in Figs. 9–11, respectively, for the three bevel angles. The increasing distortion of the plume with increasing degree of modifications, due to larger bevel angle and compensatory alteration of the secondary, is evident in these figures. Further, the centroids of the jet plumes are located close to the jet centerline (x axis). Thus, the ability to control the jet plume for any given beveled primary nozzle with a suitable offsetting effect induced by the modified secondary nozzle has been

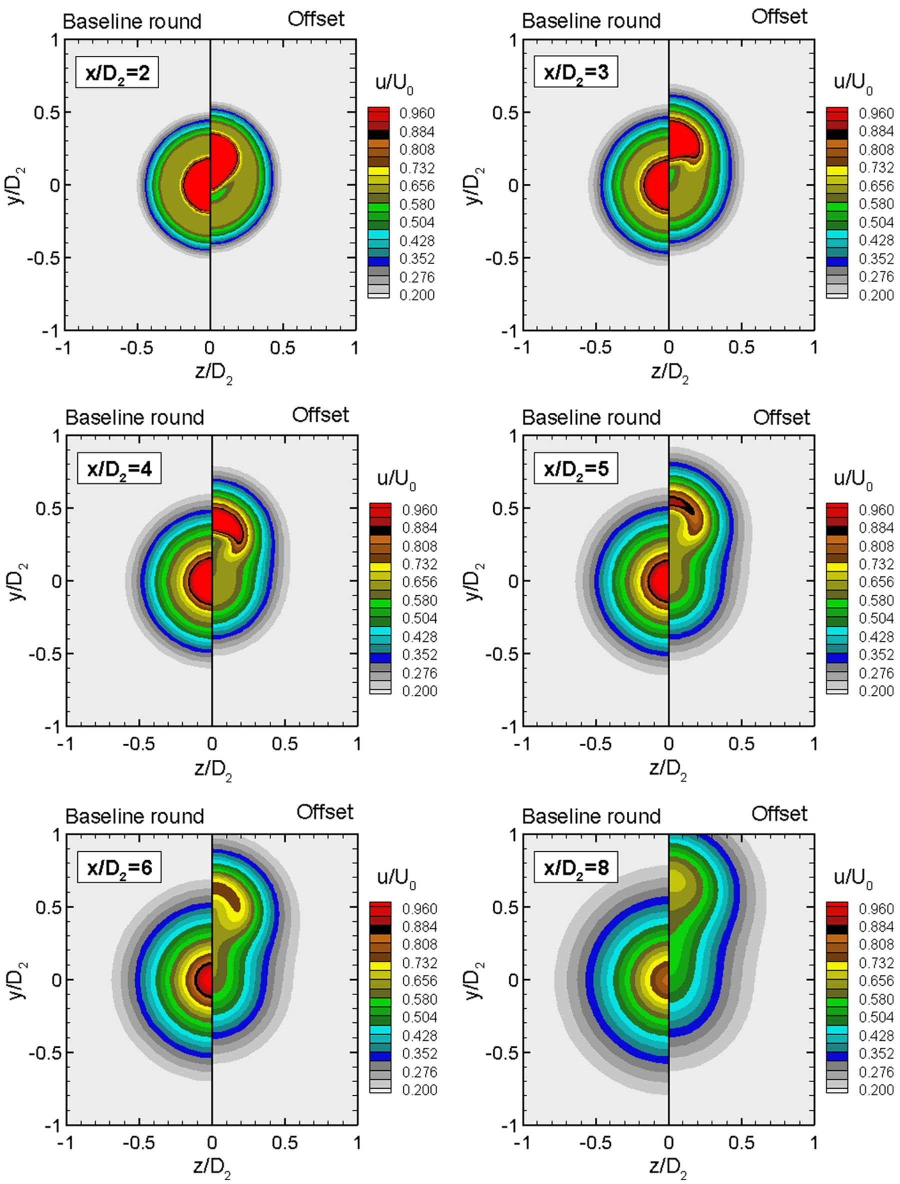

Fig. 6 Streamwise velocity in cross-sectional plane. $\mathrm{NPR}_p = \mathrm{NPR}_s = 1.8$, $T_p/T_a = 2.37$, $T_s/T_a = 1.0$, and $M_t = 0.20$. Left: baseline (round + round); right: bevel45 + round.

demonstrated. The noise characteristics of these nozzle geometries will now be evaluated.

VI. Experimental Results

The salient results from the aeroacoustic test program are presented in this section. First, the aerodynamic performance of the various nozzle combinations is presented and discussed. The acoustic results are then highlighted using several noise metrics.

A. Aerodynamic Performance

Particular attention is paid to the thrust measurements, given the importance of quantifying and controlling the plume deflection angle with the various nozzle geometries. The force balance was calibrated by applying a known force and measuring the response of the balance. The applied force was incremented by 100 lbf, starting from 0 to 1400 lbf. Then, the applied load was decreased 100 lbf stepwise, so as to document hysteresis effects, if any. This exercise was carried out twice, the first time before the start of the test and the second time after the completion of the test. Figure 12 shows the calibration curve; there are two sets of circles (pretest calibration) and two sets of triangles (post-test calibration). The straight line is the ideal response, with a 45 deg slope. As seen, there is excellent linear response, and the average error for the calibration is $\pm 0.13\%$. In general, the maximum error in the thrust measurements can be taken to be less than $\pm 0.20\%$, although it can be actually lower. Additional information may be found in Sec. III.B of [28]. The measured thrust is used to calculate the thrust coefficient using the gas dynamic equations and standard procedure. This procedure involves the calculation of the ideal jet velocities in the two streams, together with the measured mass flow rates for the determination of the ideal thrust. The thrust coefficient is the ratio of the measured thrust divided by the ideal thrust.

First, it is verified that the measured mass flow rates for the baseline and beveled nozzles are very close. This step is essential for noise differences to be meaningful. Figure 13 shows the variation of the corrected mass flow rate with NPR. The corrected mass flow rate at standard ambient conditions is calculated from the measured mass flow rate using the usual definition. The trends for the beveled nozzles are very close to that of the baseline round nozzle. This level of agreement is deemed to be acceptable for this proof-of-concept test, and, therefore, any fine-tuning of the plug position is not carried out in the interest of test time. The plume deflection angle is calculated from the measured axial and normal forces. The sign convention for the deflection angle is as follows: when the deflection

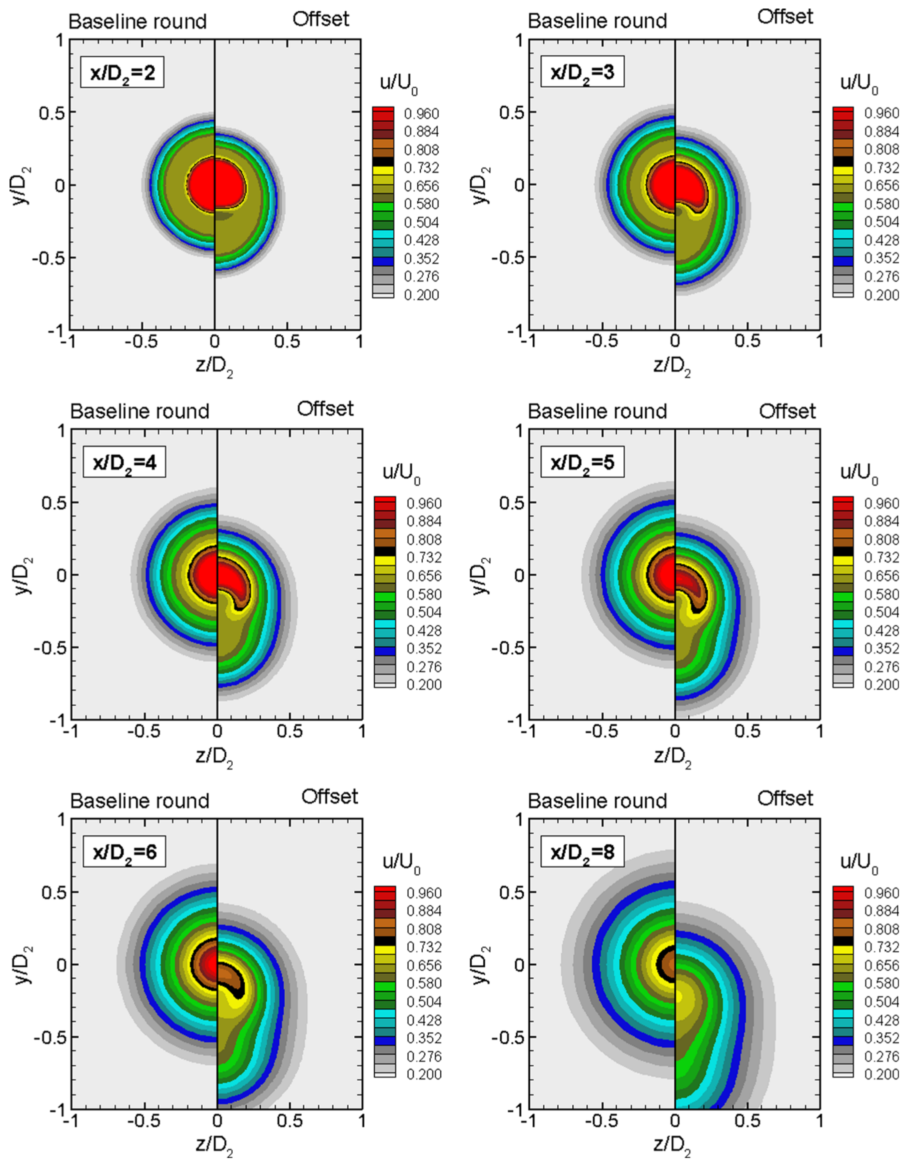

Fig. 7 Streamwise velocity in cross-sectional plane. $NPR_p = NPR_s = 1.8$, $T_p/T_a = 2.37$, $T_s/T_a = 1.0$, and $M_t = 0.20$. Left: baseline (round + round); right: round + modified B.

is toward the short lip of the beveled nozzle, the angle is taken to be positive; when the deflection is toward the long lip, it is negative. Figure 14 shows the measured deflection angles for all the nozzle geometries tested at maximum takeoff power: $NPR_p = 1.71$, $T_p/T_a = 3.16$, $NPR_s = 1.76$, $T_s/T_a = 1.24$. The modified secondary nozzles, in conjunction with the round primary nozzle, deflect the plume downward; the deflection angle is larger for the stronger modification, as expected. The deflections due to the beveled nozzles, in conjunction with the round secondary nozzles, increase progressively with increasing bevel angle: from ~ 1 deg for bevel 18 to ~ 2.2 deg for bevel 36. Again, the expected trends are manifested in the measurements. The vertical chain lines demarcate the different beveled nozzles in Fig. 14. The combinations of the modified nozzles with the bevels produce the desired reduction in the plume deflection angle: the stronger the modification to the secondary, the larger the reduction in the deflection angle. Similar trends for plume deflection are observed in Fig. 15 at cutback power: $NPR_p = 1.38$, $T_p/T_a = 2.74$, $NPR_s = 1.56$, $T_s/T_a = 1.16$. The measured trends are in accord with the plume characteristics observed in the RANS simulations, and confirm the efficacy of the design philosophy. It is not at all surprising that bevel 36 produces the maximum plume deflection. However, that is not the optimum bevel angle for noise, as will be seen. In general, the values of the deflection angle are within $\pm \sim 1.5$ deg. The cosine of 1.5 deg is 0.99966, so that the thrust loss is negligible. It is important to keep in mind that there is no single-point design for a particular bevel angle; rather, combinations of bevel angles and modifications to the secondary are evaluated so as to create a database. The effect of the normal force due to plume deflection must be considered in practical applications.

The propulsive performance of the various nozzle geometries is next assessed. It is easier to observe the effect of nozzle modifications through the examination of the difference in thrust coefficient relative to that of the baseline nozzle system. Figures 16 and 17 show such variations at maximum takeoff power and cutback power, respectively. The nozzle with the largest bevel angle produces the largest thrust loss relative to the baseline. In general, the combinations of bevel 24 and bevel 30 with the modified nozzles lead to relatively low thrust degradation, nearly within the experimental measurement error. These results suggest that it should be possible in theory to design a dual-stream nozzle system with acceptable performance penalty for a desired beveled primary nozzle.

B. Acoustics

The acoustic performance of the various nozzle geometries is assessed now. The accuracy of the spectral measurements is

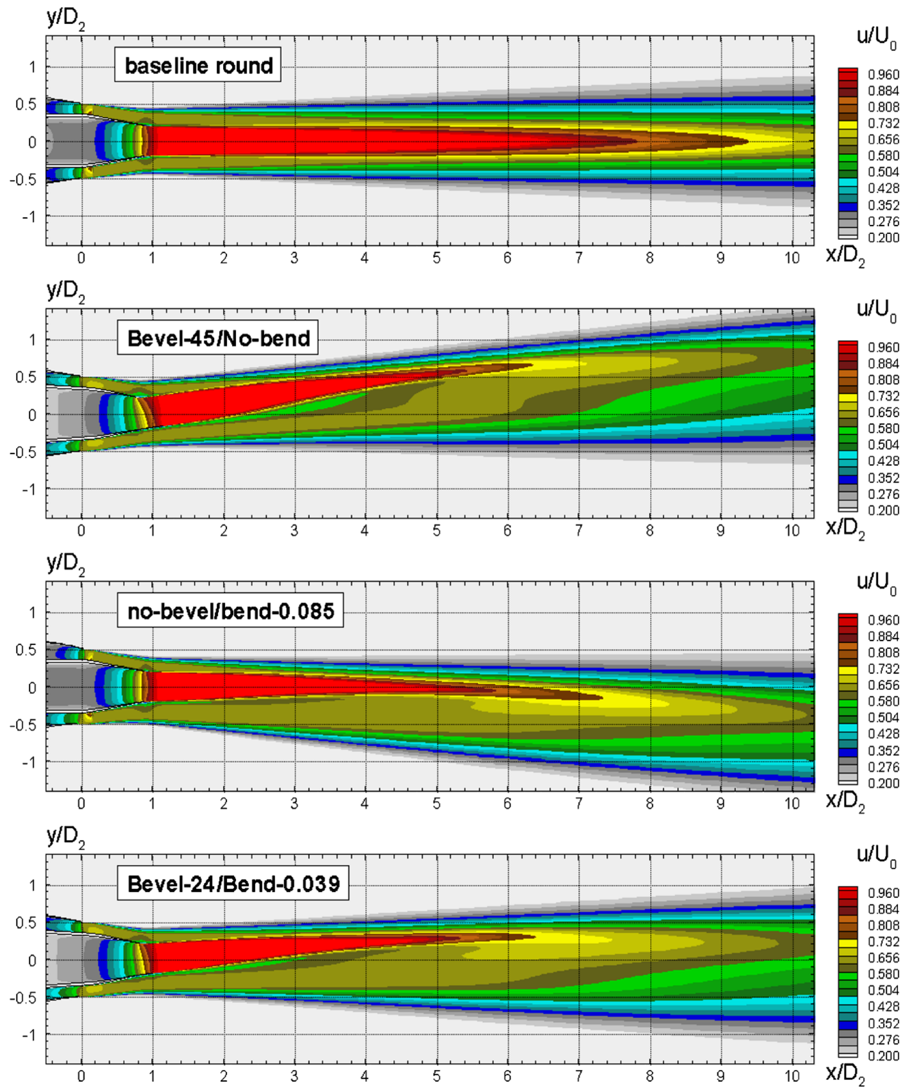

Fig. 8 Axial variation of streamwise velocity in symmetry plane of jet. $NPR_p = NPR_s = 1.8$, $T_p/T_a = 2.37$, $T_s/T_a = 1.0$, and $M_t = 0.20$. a) Baseline, b) bevel45 + round, c) round + modified B, and d) bevel24 + modified C.

within $\pm \sim 0.5$ dB or better, as demonstrated in Viswanathan [28,29]. The as-measured spectra are converted to lossless conditions for comparisons at model scale. The method proposed by Shields and Bass [30] is used to calculate the atmospheric absorption coefficients, which are frequency dependent. For the test conditions with forward flight, the acoustic rays from the jet are subject to two effects: 1) convection in the downstream direction due to the freestream, and 2) refraction due to the tunnel shear layer. The changes in the spectral amplitude and the radiation angle due to the coflow have been calculated using the procedure developed by Amiet [31,32]. The geometries of the jet and the wind tunnel are used to calculate the actual distance traveled by the acoustic rays. The distributed sources of the jet are assumed to be represented by a point source located at the center of the nozzle exit plane. It has been shown in Viswanathan [33,34] that the microphones are indeed located in the true acoustic and geometric far field for the nozzles used here. For the wind-on case, the proper values of the atmospheric attenuations inside and outside the tunnel flow are used. The resulting spectra are interpolated to fixed observer angles; these observer angles are the same microphone angles for the static case, described in Sec. IV. For engine-scale comparisons, the model-scale spectra are extrapolated to full-scale conditions with a level flight for the aircraft at a fixed altitude of 1000 ft. Lossless spectral comparisons as functions of raw frequency in hertz are presented in the following figures.

1. Jets in Static Environment

The efficacy of the modifications to the secondary nozzle vis-à-vis noise reduction is first evaluated. For the sake of clarity, the definitions of various angles, viz., polar (χ), azimuthal (ϕ), and bevel angle (θ) are identified with a sketch in Fig. 18. Spectral comparisons at four polar angles of 90, 130, 140, and 150 deg are shown in the following figures; an examination of a large set of data indicates that the changes to the spectra at the lower polar angles are relatively minor, and the spectral changes at 90 deg can be taken to be representative of the trends at all the lower polar angles in the forward quadrant. Figure 19 presents a comparison of the spectra obtained with the baseline (round + round), round + MF1, round + MF2, and bevel 24 + round; the jet conditions are $NPR_p = 1.55$, $T_p/T_a = 3.0$, $NPR_s = 1.71$, $T_s/T_a = 1.21$. The azimuthal angle (ϕ) is 0 deg, as when the observer is directly below the aircraft. There are only minor changes at 90 deg. Both the modified secondary nozzles yield noise reductions in the peak radiation sector at large aft angles. Thus, it is verified that the modified secondary nozzles do provide a noise benefit in the peak radiation sector. But, the magnitude of reduction is much smaller than what is obtained with bevel 24. When the engine power is increased to $NPR_p = 1.71$, $T_p/T_a = 3.16$, $NPR_s = 1.76$, $T_s/T_a = 1.24$ in Fig. 20, the noise reductions due to MF1 and MF2 are enhanced slightly; however, the larger magnitude of reduction at the higher power for the bevel 24 is not observed for the modifications to the secondary nozzle.

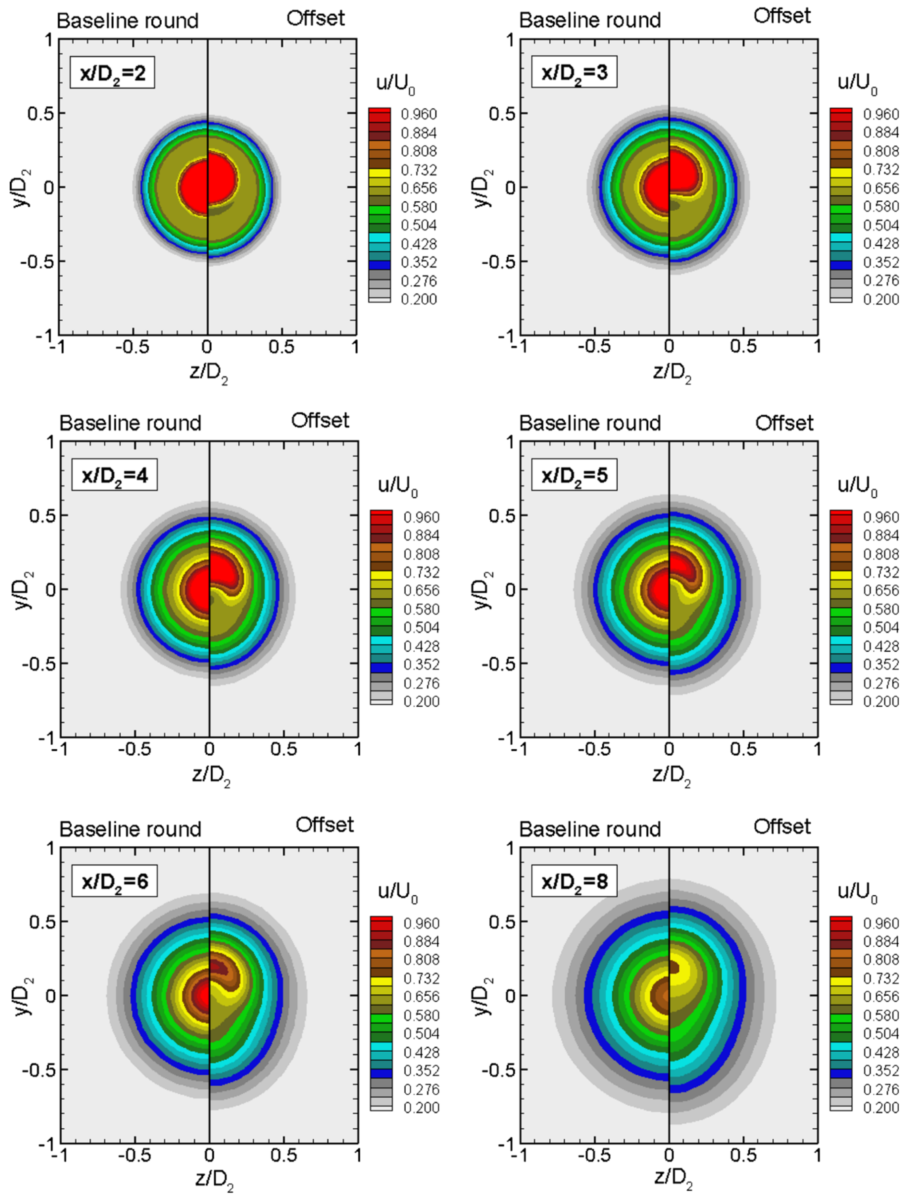

Fig. 9 Streamwise velocity in cross-sectional plane. $NPR_p = NPR_s = 1.8$, $T_p/T_a = 2.37$, $T_s/T_a = 1.0$, and $M_t = 0.20$. Left: baseline (round + round); right: bevel15 + modified D.

The reason for the lower noise benefit obtained with the modifications to the secondary becomes apparent when the azimuthal variation is examined. Figures 21 and 22 show spectral variations at the same four polar angles, but at $\phi = 0$, 30, and 60 deg, for the round + MF2 and bevel24 + round, respectively. The jet operating conditions are $NPR_p = 1.71$, $T_p/T_a = 3.16$, $NPR_s = 1.76$, $T_s/T_a = 1.24$. There are some blips in the spectra at 150 deg at ∼250 Hz, for the microphones at azimuthal angles of 30 and 60 deg; these blips are caused by reflections from the exhaust collector, as explained by Viswanathan [29]. Note that for the microphone arrays at constant fixed sideline distance, the axial microphone locations at 150 deg are closer to the exhaust collector. These tones should be ignored, as they are not part of the changes to the noise due to nozzle modifications. First of all, the noise level increases in the peak radiation sector with increasing azimuthal angle for both geometries. It is also clear that the degree of azimuthal variation introduced by MF2 is much less pronounced (∼2 to ∼3 dB) when compared with that due to bevel 24 (∼5 to ∼6 dB). One could infer then that the lower noise benefit observed in Figs. 19 and 20 is due to the weaker effect of MF1 and MF2 in introducing azimuthal variations in the spectra.

The noise benefit obtained with the different bevel nozzles (bevel angles of 24, 30, and 36 deg) is quantified in Figs. 23 and 24, for the two power settings of $NPR_p = 1.55$, $T_p/T_a = 3.0$, $NPR_s = 1.71$, $T_s/T_a = 1.21$ and $NPR_p = 1.71$, $T_p/T_a = 3.16$, $NPR_s = 1.76$, $T_s/T_a = 1.24$, respectively. In general, the noise benefit increases with increasing bevel angle; furthermore, the magnitude of noise benefit for a given bevel angle is larger for the higher power setting, with increased primary jet velocity. The observed trends at static conditions in the current test are consistent with the trends reported by Viswanathan [18].

2. *Jets in Forward Flight*

The effects of forward flight on noise of various geometries are assessed next. As for the static case, the noise potential of the modified secondary nozzles is examined first. Figure 25 presents a comparison of the spectra obtained with the baseline (round + round), round + MF1, round + MF2, and bevel24+ round; the jet conditions are $NPR_p = 1.62$, $T_p/T_a = 3.07$, $NPR_s = 1.74$, $T_s/T_a = 1.22$. The azimuthal angle (ϕ) is 0 deg and the freestream Mach number $M_t = 0.20$. The spectral changes are again minor at 90 deg. In the peak directions, all the modified nozzles yield noise reductions. It is also worth pointing out that there is no increase at the higher frequencies, both for the static and wind-on cases. The power setting is increased to $NPR_p = 1.71$,

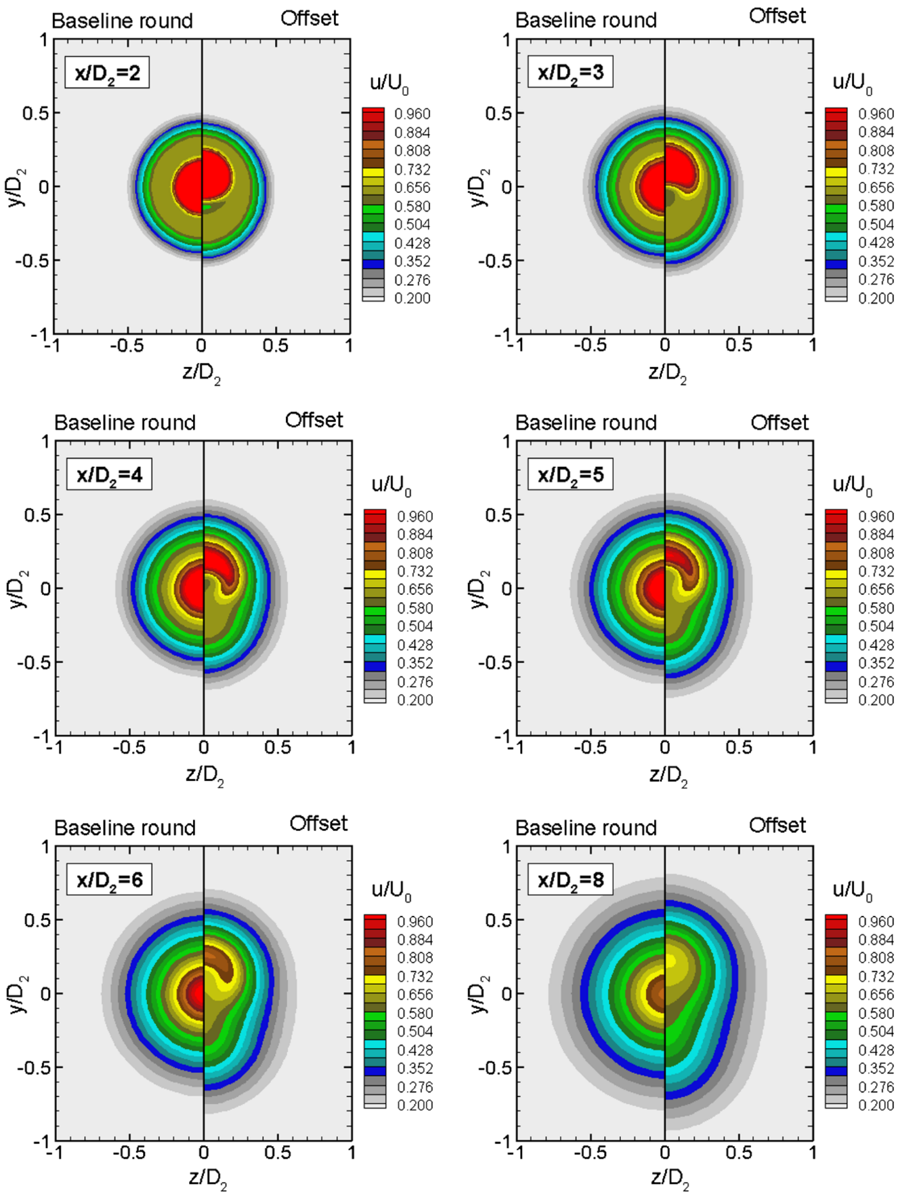

Fig. 10 Streamwise velocity in cross-sectional plane. $NPR_p = NPR_s = 1.8$, $T_p/T_a = 2.37$, $T_s/T_a = 1.0$, and $M_t = 0.20$. Left: baseline (round + round); right: bevel20 + modified E.

$T_p/T_a = 3.16$, $NPR_s = 1.76$, $T_s/T_a = 1.24$ in Fig. 26. Comparable spectral trends, but with larger noise reductions, are observed at this higher power. Once again, bevel 24 provides a larger noise benefit. Therefore, it is established that the design philosophy for the secondary-nozzle modifications, in which the flow cross sections resemble those due to the primary bevel, provides noise benefit both for jets in static conditions and in the presence of a forward flight stream.

The noise characteristics of geometries with modifications to both nozzles are examined now. Spectral comparisons of the baseline (round + round) with bevel24 + round and bevel24 + MF1 are shown in Fig. 27. The jet operating conditions are $NPR_p = 1.55$, $T_p/T_a = 3.0$, $NPR_s = 1.71$, $T_s/T_a = 1.21$. The azimuthal angle (ϕ) is 0 deg and the freestream Mach number $M_t = 0.20$. At 90 deg, there is negligible change. At lower polar angles (not shown), there is a slight increase in level. In the peak radiation sector, there is a ~3 to ~4 dB reduction in level over a large frequency range near the spectral peak, without increased levels at the higher frequencies. An immediate observation is the following: most of the noise benefit is provided by bevel 24, with the addition of MF1 resulting in very minor changes.

Another comparison of the baseline with bevel30 + round and bevel30 + MF1 is shown in Fig. 28, at the higher power setting of $NPR_p = 1.71$, $T_p/T_a = 3.16$, $NPR_s = 1.76$, $T_s/T_a = 1.24$. The azimuthal angle (ϕ) is 0 deg and the freestream Mach number $M_t = 0.20$. The observed spectral trends are similar to those seen in Fig. 27. There is a larger noise benefit at the aft angles. Again, most of the noise benefit is provided by bevel 30. The freestream Mach number is increased to 0.28 in Fig. 29. The tail up at the lower frequencies is due to contamination from the tunnel noise floor and is not related to the noise from the jet. At this higher M_t, there is noise increase at 90 deg and at the lower angles; as we move aft, spectral reductions are obtained. So far, attention has been restricted to $\phi = 0$ deg. Now, the spectral characteristics at other azimuthal angles are examined. Figures 30 and 31 depict comparisons for the same operating conditions, but at $\phi = 30$ and 60 deg, respectively. At $\phi = 30$ deg in Fig. 30, there is a slight increase in level at 90 deg; there is still a larger noise reduction at the aft angles. At $\phi = 60$ deg in Fig. 31, the angular range over which noise reduction is observed is drastically reduced; even at 130 deg, there is an increase in levels at the higher frequencies, although there is some reduction at the lower frequencies. Similar trends are observed at other jet conditions (not shown). It is important to keep in mind that the nozzle designs investigated here are directional in character, in that noise reductions are obtained over a certain angular sector in the azimuthal plane. The benefit peaks at $\phi = 0$ deg and gradually diminishes with increase in

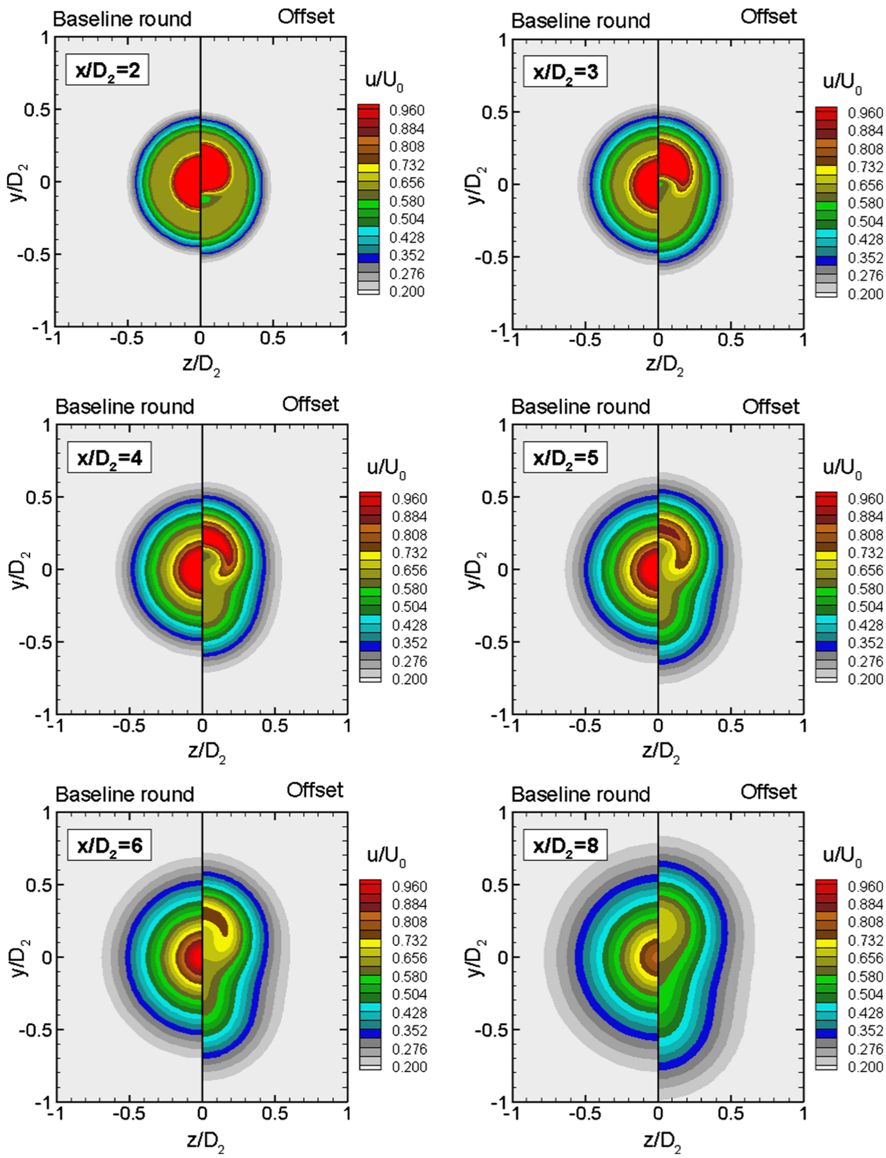

Fig. 11 Streamwise velocity in cross-sectional plane. $\mathrm{NPR}_p = \mathrm{NPR}_s = 1.8$, $T_p/T_a = 2.37$, $T_s/T_a = 1.0$, and $M_t = 0.20$. Left: baseline (round + round); right: bevel24 + modified C.

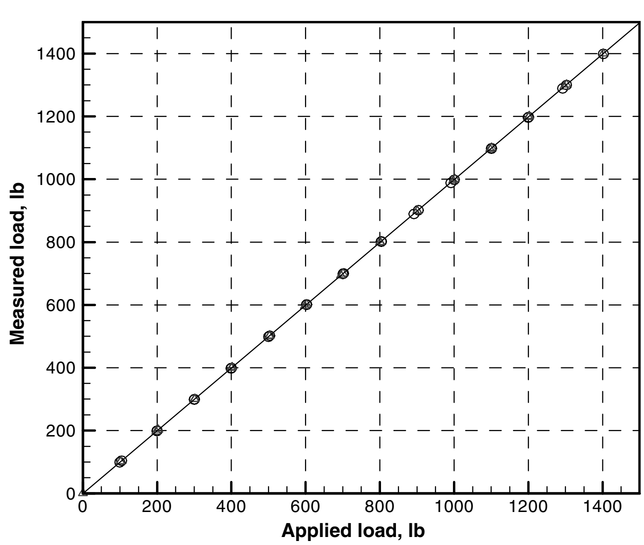

Fig. 12 Calibration of force balance showing measured load vs applied load. o: pretest; Δ: post-test.

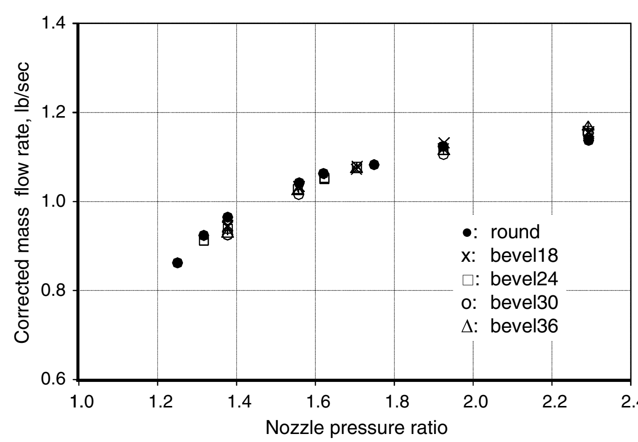

Fig. 13 Comparison of corrected mass flow rates for the baseline and beveled nozzles.

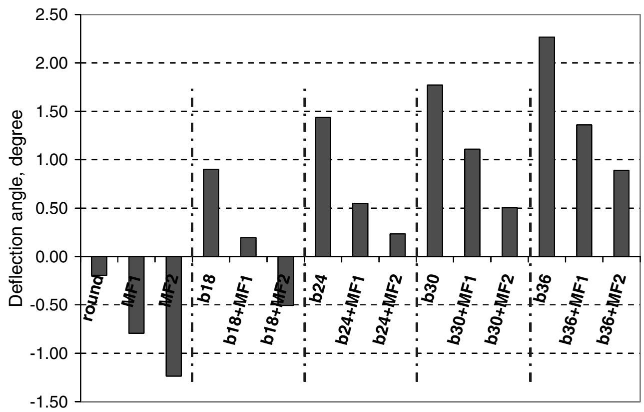

Fig. 14 Plume deflection angle for different nozzle geometries. $NPR_p = 1.71$, $T_p/T_a = 3.16$, $NPR_s = 1.76$, $T_s/T_a = 1.24$.

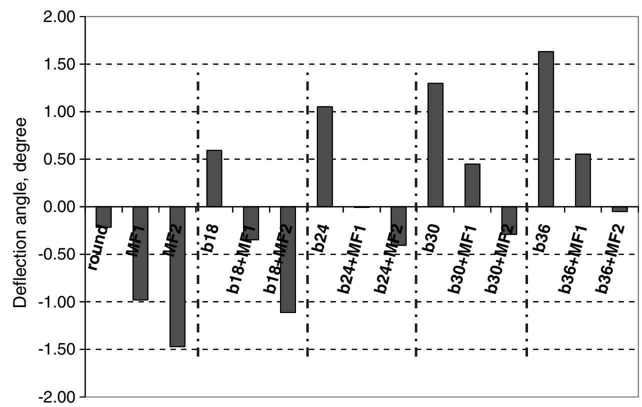

Fig. 15 Plume deflection angle for different nozzle geometries. $NPR_p = 1.38$, $T_p/T_a = 2.74$, $NPR_s = 1.56$, $T_s/T_a = 1.16$.

azimuthal angle. Such behavior has been reported by Viswanathan [18] for the primary bevel with a round secondary; given the minor spectral modifications introduced by the addition of a modified secondary nozzle, perhaps it should not be surprising that similar trends are observed for the combination of beveled primary with modified secondary nozzle.

Finally, the noise benefits are quantified at engine scale. As already noted, the measured spectra are extrapolated to engine scale, with a steady level flight for the airplane at an altitude of 1000 ft. The variation of the perceived noise level (PNL, PNdB) with radiation angle provides a composite picture of the noise characteristics. Such a variation is presented in Fig. 32 for the baseline, round + MF1, and bevel24 + MF2. The jet operating conditions are $NPR_p = 1.62$, $T_p/T_a = 3.07$, $NPR_s = 1.74$, $T_s/T_a = 1.22$. The azimuthal angle $\phi = 0$ deg and the freestream Mach number $M_t = 0.20$. The modified nozzle MF1 by itself provides a slight reduction in PNL at the aft angles. The combination of bevel24 + MF2 results in a slight increase of ~1 dB at the lower polar angles; however, there is significant noise reduction of ~3 to ~4 dB at large aft angles. The benefits in the EPNL (EPNdB) relative to the baseline are 0.54 and 1.2 dB, respectively, for these two modified geometries. Another sample variation of PNL is shown in Fig. 33 for the baseline, bevel30 + round, and bevel30 + MF1. The jet operating conditions are $NPR_p = 1.71$, $T_p/T_a = 3.16$, $NPR_s = 1.76$, $T_s/T_a = 1.24$. The azimuthal angle $\phi = 0$ deg and the freestream Mach number $M_t = 0.20$. At this higher power setting, the reduction in PNL is substantial in the aft quadrant, for polar angles ≥ 120 deg. These trends are consistent with the spectral variations shown in Fig. 29. Again, there is a slight increase in level at the lower polar angles. The noise benefits in EPNL for the two geometries are 2.0 and 1.96 EPNdB, respectively.

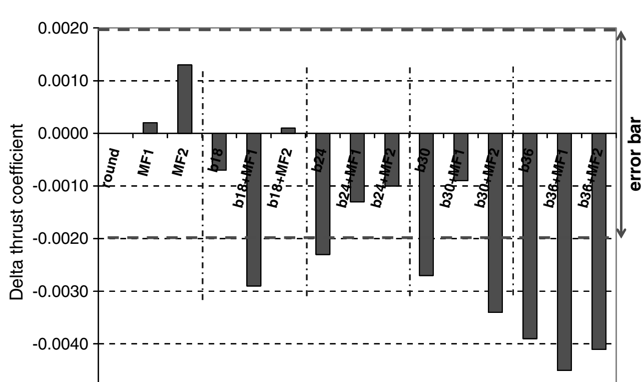

Fig. 16 Difference in thrust performance relative to baseline nozzle geometry. $NPR_p = 1.71$, $T_p/T_a = 3.16$, $NPR_s = 1.76$, $T_s/T_a = 1.24$.

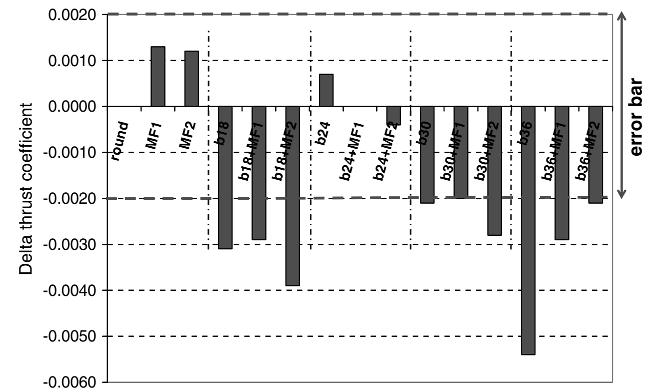

Fig. 17 Difference in thrust performance relative to baseline nozzle geometry. $NPR_p = 1.38$, $T_p/T_a = 2.74$, $NPR_s = 1.56$, $T_s/T_a = 1.16$.

The noise benefit, relative to the baseline, for all the geometries is presented at three freestream Mach numbers of 0.0, 0.20, and 0.28 in Fig. 34. The jet operating conditions are $NPR_p = 1.71$, $T_p/T_a = 3.16$, $NPR_s = 1.76$, $T_s/T_a = 1.24$. The azimuthal angle $\phi = 0$ deg. For the static case, the noise benefit increases with increasing bevel angle; there is a reduction of 2.65 EPNdB for bevel 36. This trend was observed by Viswanathan [18] as well. However, the introduction of a flight stream changes the achieved benefit for the different geometries. First of all, the benefit is reduced when there is a flight stream. This effect becomes more pronounced with increasing M_t. For example, for bevel30 + MF1, the noise reductions are 2.48, 1.96, and 1.22 EPNdB, respectively, at the three flight Mach numbers. A combined analysis of thrust performance and noise benefit, over a larger range of jet operating conditions, reveals that the optimum bevel angle is somewhere between 24 and 30 deg. The combinations of the modified secondary nozzles with the bevel 24 and bevel 30 primary nozzles provide the most noise benefit over a wide range of flight Mach numbers and lower thrust degradation. The large database generated in the current study may be used in

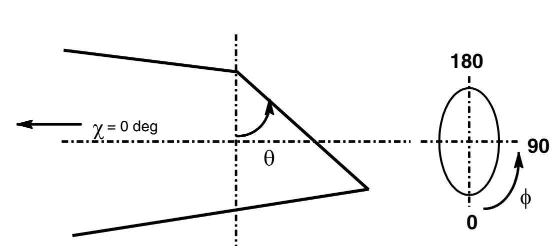

Fig. 18 Conceptual sketch of the beveled nozzle and the measurement convention for the bevel angle (θ), the polar angle (χ), and the azimuthal angle (ϕ).

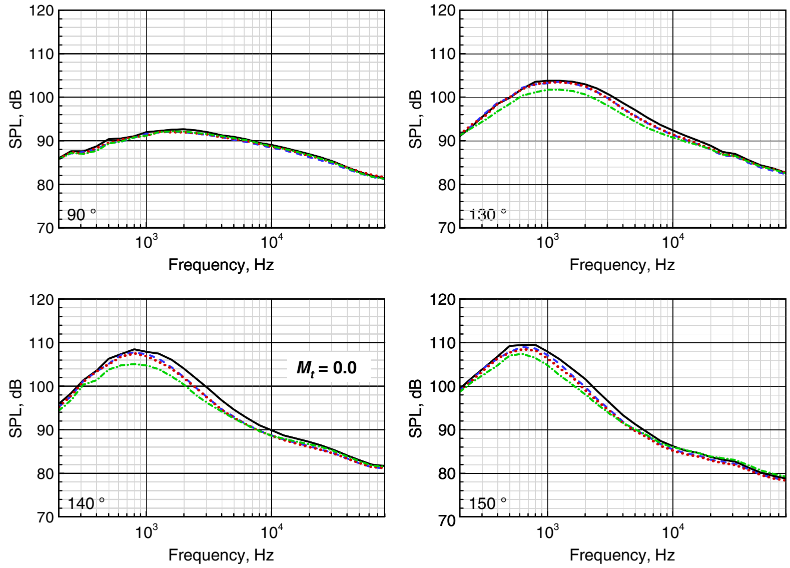

Fig. 19 Spectral changes due to nozzle modifications. $\mathrm{NPR}_p = 1.55$, $T_p/T_a = 3.0$, $\mathrm{NPR}_s = 1.71$, $T_s/T_a = 1.21$. Black (solid): baseline; blue (dashed): round + MF1; red (dotted): round + MF2; green (chain): bevel24 + round. $\phi = 0$ deg.

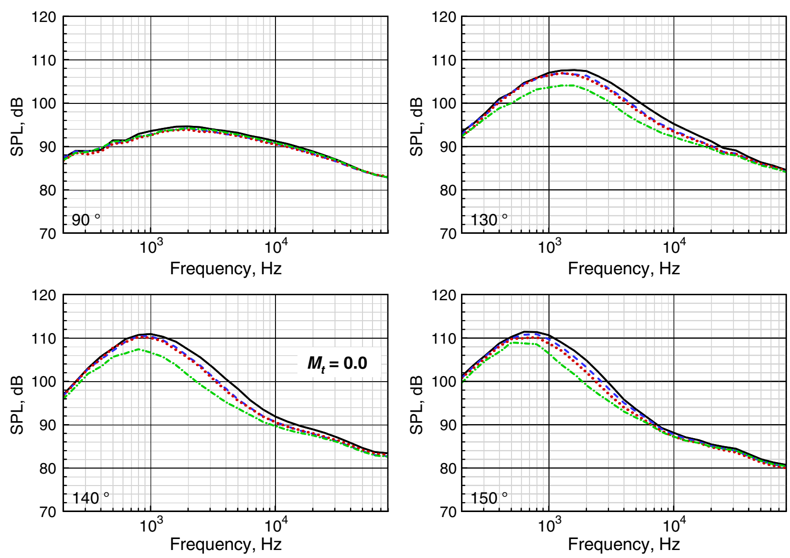

Fig. 20 Spectral changes due to nozzle modifications. $\mathrm{NPR}_p = 1.71$, $T_p/T_a = 3.16$, $\mathrm{NPR}_s = 1.76$, $T_s/T_a = 1.24$. Black (solid): baseline; blue (dashed): round + MF1; red (dotted): round + MF2; green (chain): bevel24 + round. $\phi = 0$ deg.

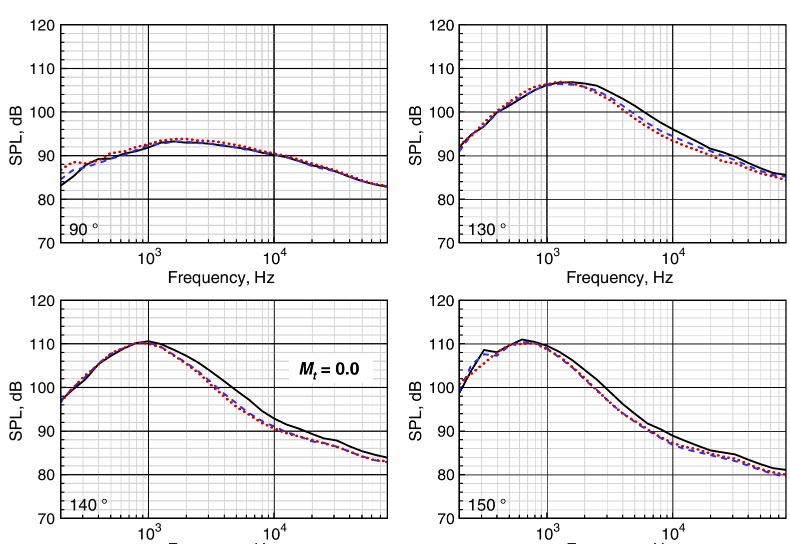

Fig. 21 Azimuthal variation. $\mathrm{NPR}_p = 1.71$, $T_p/T_a = 3.16$, $\mathrm{NPR}_s = 1.76$, $T_s/T_a = 1.24$. Round + MF2. Black (solid): $\phi = 60$ deg; blue (dashed): $\phi = 30$ deg; red (dotted): $\phi = 0$ deg.

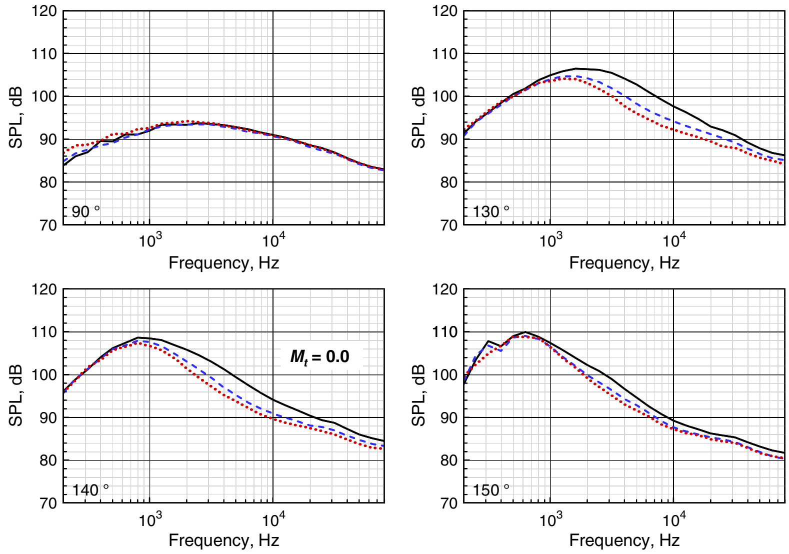

Fig. 22 Azimuthal variation. $NPR_p = 1.71$, $T_p/T_a = 3.16$, $NPR_s = 1.76$, $T_s/T_a = 1.24$. Bevel24 + round. Black (solid): $\phi = 60$ deg; blue (dashed): $\phi = 30$ deg; red (dotted): $\phi = 0$ deg.

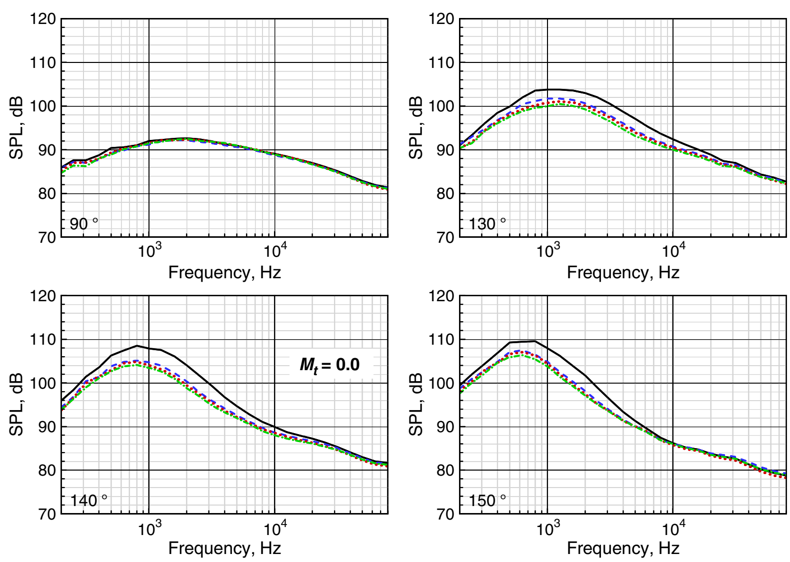

Fig. 23 Spectral changes due to nozzle modifications. $NPR_p = 1.55$, $T_p/T_a = 3.0$, $NPR_s = 1.71$, $T_s/T_a = 1.21$. Black (solid): baseline; blue (dashed): bevel24 + round; red (dotted): bevel30 + round; green (chain): bevel36 + round. $\phi = 0$ deg.

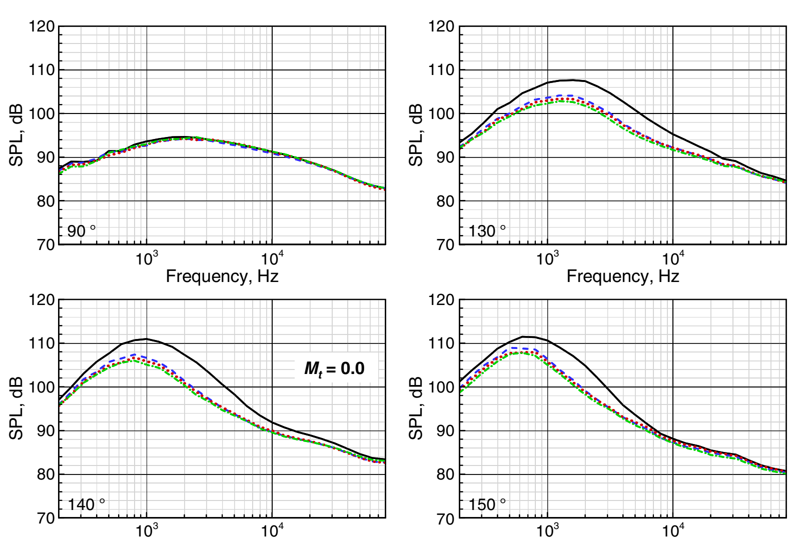

Fig. 24 Spectral changes due to nozzle modifications. $NPR_p = 1.71$, $T_p/T_a = 3.16$, $NPR_s = 1.76$, $T_s/T_a = 1.24$. Black (solid): baseline; blue (dashed): bevel24 + round; red (dotted): bevel30 + round; green (chain): bevel36 + round. $\phi = 0$ deg.

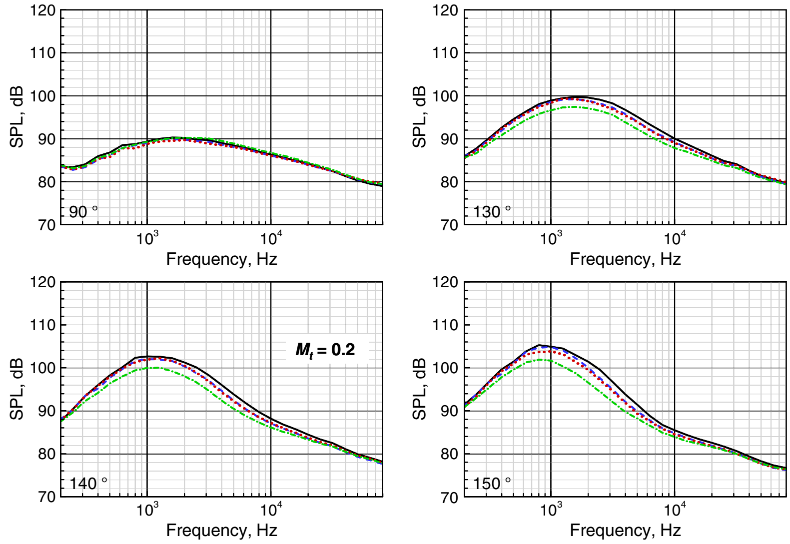

Fig. 25 Spectral changes due to nozzle modifications. $\mathrm{NPR}_p = 1.62$, $T_p/T_a = 3.07$, $\mathrm{NPR}_s = 1.74$, $T_s/T_a = 1.22$. Black (solid): baseline; blue (dashed): round + MF1; red (dotted): round + MF2; green (chain): bevel24 + round. $\phi = 0$ deg.

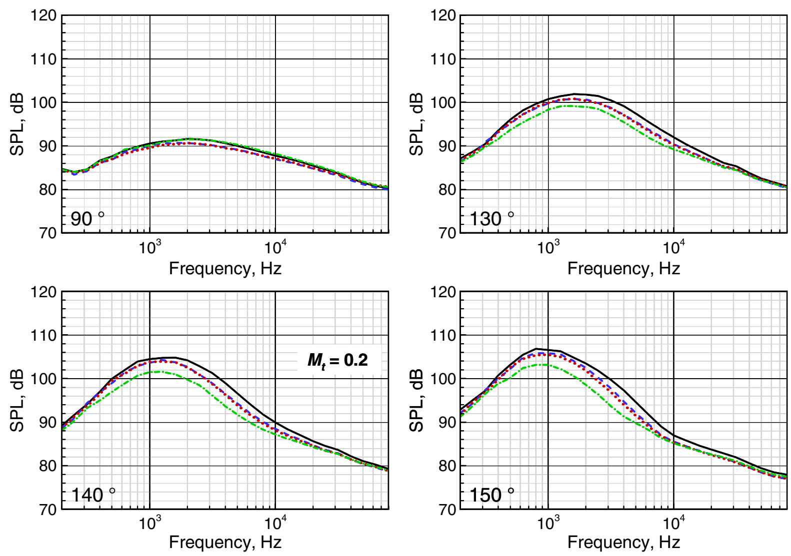

Fig. 26 Spectral changes due to nozzle modifications. $\mathrm{NPR}_p = 1.71$, $T_p/T_a = 3.16$, $\mathrm{NPR}_s = 1.76$, $T_s/T_a = 1.24$. Black (solid): baseline; blue (dashed): round + MF1; red (dotted): round + MF2; green (chain): bevel24 + round. $\phi = 0$ deg.

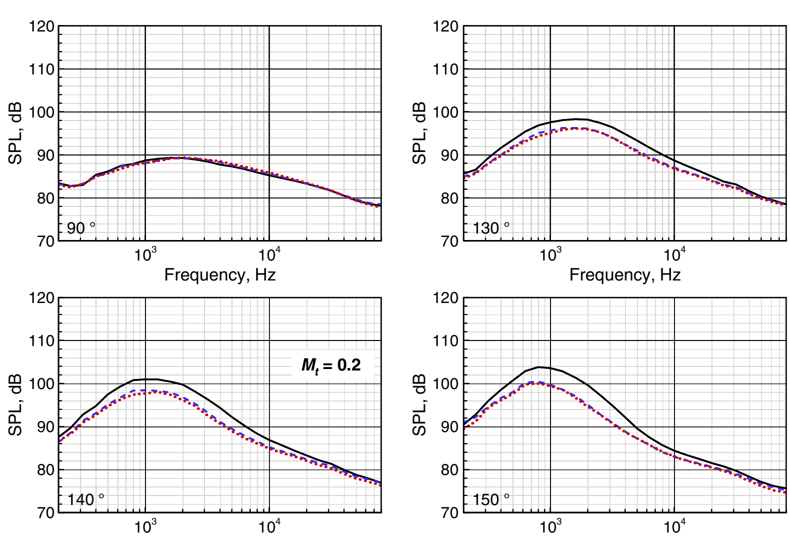

Fig. 27 Spectral changes due to nozzle modifications. $\mathrm{NPR}_p = 1.55$, $T_p/T_a = 3.0$, $\mathrm{NPR}_s = 1.71$, $T_s/T_a = 1.21$. Black (solid): baseline; blue (dashed): bevel24 + round; red (dotted): bevel24 + MF1. $\phi = 0$ deg.

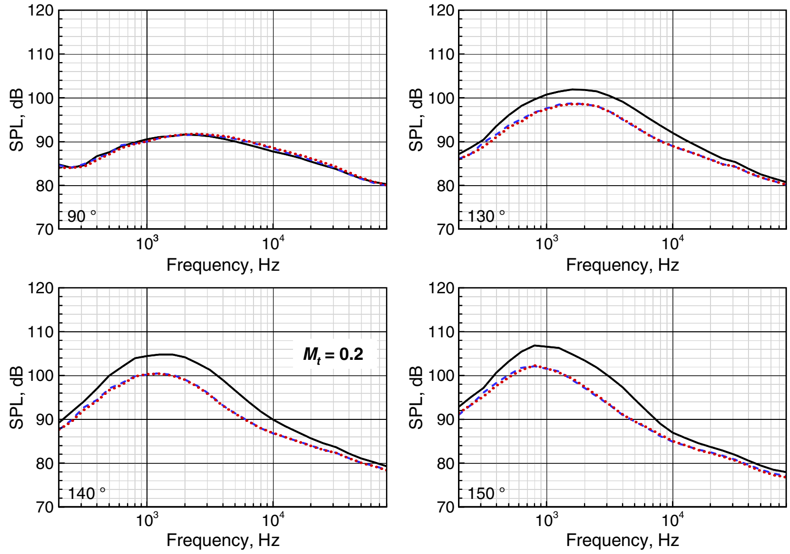

Fig. 28 Spectral changes due to nozzle modifications. $\mathrm{NPR}_p = 1.71$, $T_p/T_a = 3.16$, $\mathrm{NPR}_s = 1.76$, $T_s/T_a = 1.24$. Black (solid): baseline; blue (dashed): bevel30 + round; red (dotted): bevel30 + MF1. $\phi = 0$ deg.

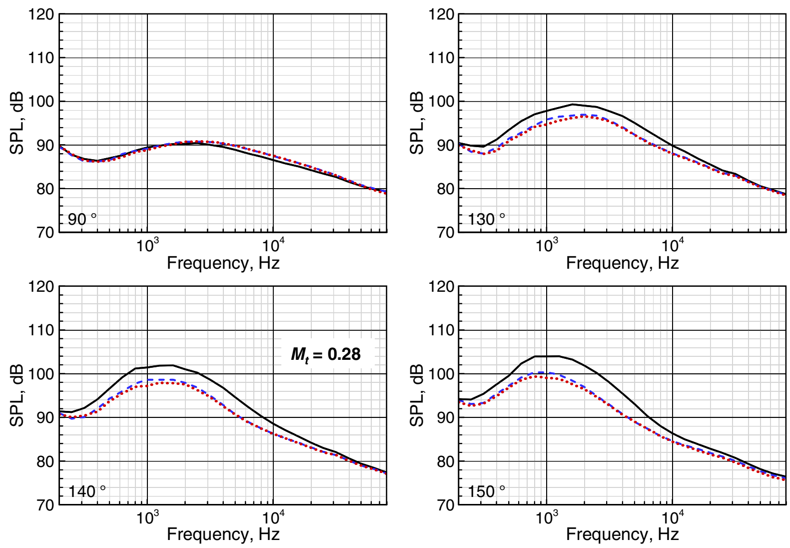

Fig. 29 Spectral changes due to nozzle modifications. $\mathrm{NPR}_p = 1.71$, $T_p/T_a = 3.16$, $\mathrm{NPR}_s = 1.76$, $T_s/T_a = 1.24$. Black (solid): baseline; blue (dashed): bevel30 + round; red (dotted): bevel30 + MF1. $\phi = 0$ deg.

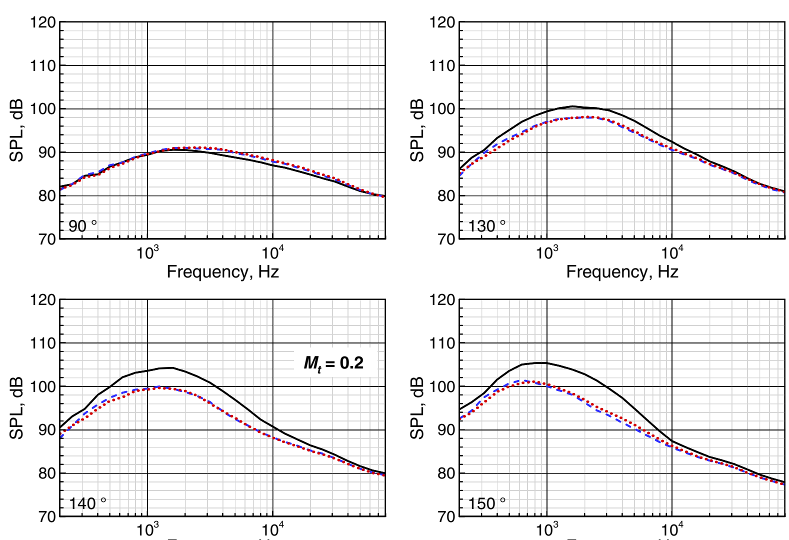

Fig. 30 Spectral changes due to nozzle modifications. $\mathrm{NPR}_p = 1.71$, $T_p/T_a = 3.16$, $\mathrm{NPR}_s = 1.76$, $T_s/T_a = 1.24$. Black (solid): baseline; blue (dashed): bevel30 + round; red (dotted): bevel30 + MF1. $\phi = 30$ deg.

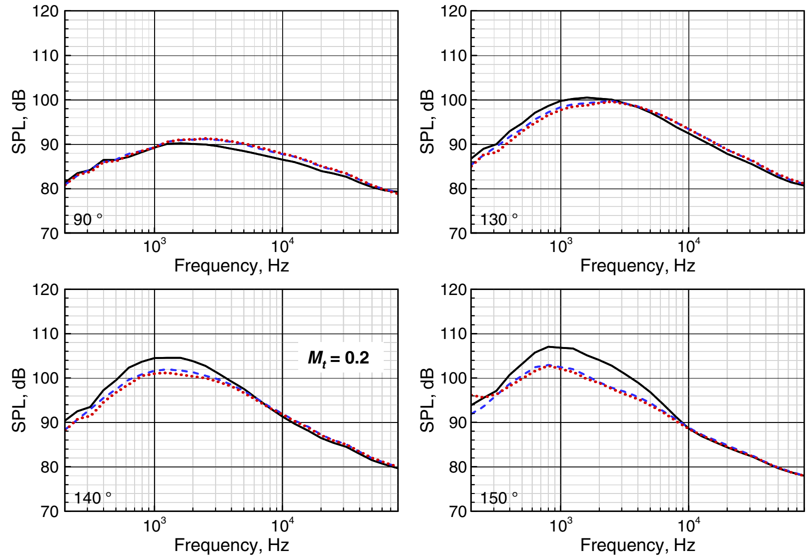

Fig. 31 Spectral changes due to nozzle modifications. $NPR_p = 1.71$, $T_p/T_a = 3.16$, $NPR_s = 1.76$, $T_s/T_a = 1.24$. Black (solid): baseline; blue (dashed): bevel30 + round; red (dotted): bevel30 + MF1. $\phi = 60$ deg.

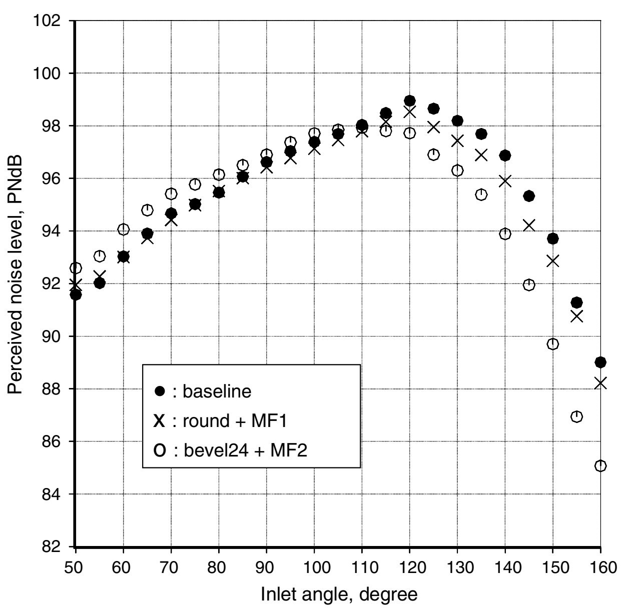

Fig. 32 Variation of PNL with angle. $NPR_p = 1.62$, $T_p/T_a = 3.07$, $NPR_s = 1.74$, $T_s/T_a = 1.22$. ●: baseline; x: round + MF1; o: bevel24 + MF2. $\phi = 0$ deg. $M_t = 0.20$.

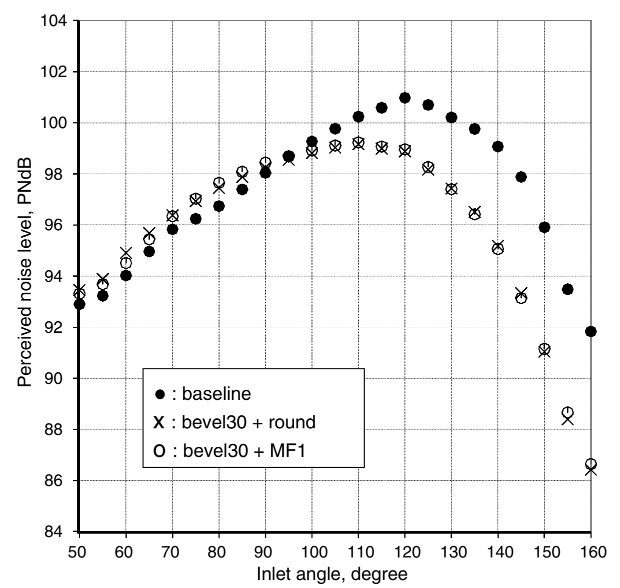

Fig. 33 Variation of PNL with angle. $NPR_p = 1.71$, $T_p/T_a = 3.16$, $NPR_s = 1.76$, $T_s/T_a = 1.24$. ●: baseline; x: bevel30 + round; o: bevel30 + MF1. $\phi = 0$ deg. $M_t = 0.20$.

conjunction with computational simulations to arrive at an optimum design for a desired bevel angle of the primary nozzle. Detailed CFD simulations of the flowfields for the best configurations and further analysis are underway, in an attempt to identify the desirable features in the flowfields.

VII. Conclusions

A methodology for designing dual-stream nozzle geometries that provides jet-noise reduction concurrently with the ability to control the orientation of the jet plume has been developed and evaluated in this joint computational and experimental investigation. The geometries consist of round primary and secondary nozzles, beveled primary nozzles, modified secondary nozzles, and combinations thereof. Computational fluid dynamics (CFD) simulations have been used to design modified secondary nozzles (in conjunction with a round primary nozzle) to produce the same cross-sectional patterns of the jet plume as produced by a beveled primary nozzle plus a round

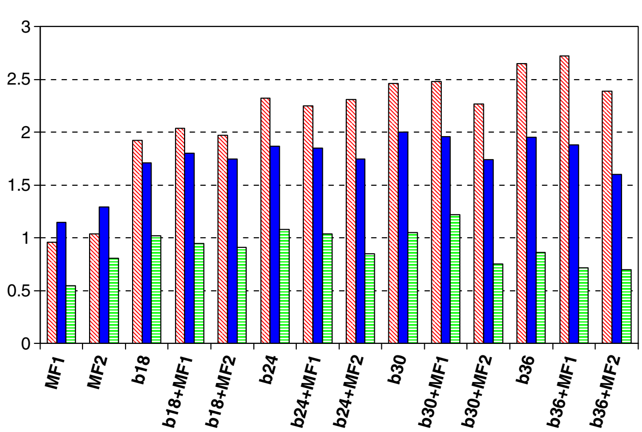

Fig. 34 EPNL benefit for various nozzle geometries. $NPR_p = 1.71$, $T_p/T_a = 3.16$, $NPR_s = 1.76$, $T_s/T_a = 1.24$. $\phi = 0$ deg. Red (slanted lines): $M_t = 0.0$; blue (solid): $M_t = 0.20$; green (horizontal lines): $M_t = 0.28$.

secondary nozzle. This objective is first demonstrated. The main difference between the two flowfields is the following: the bevel deflects the flow toward the short lip; the modified secondary deflects the flow in a diametrically opposite direction. Although the precise mechanism responsible for noise reduction by the beveled nozzle is not fully understood, it is at least possible to quantify and analyze the changes to the plume development through numerical simulations. (As an aside, it should be appreciated that the flow/noise causality is still an open question.) Such an endeavor served to underpin the design of the secondary nozzles. It has also been demonstrated through CFD that the combination of bevel + modified secondary can be precisely tailored for any desired bevel angle to eliminate the forces in a plane normal to the jet axis.

In the companion experimental study, four primary beveled nozzles with bevel angles of 18, 24, 30, and 36 deg, and two modified secondary nozzles (MF1 and MF2) have been considered. MF1 produces a weaker deflection and MF2 a stronger deflection in a direction opposite to those of the beveled nozzles. Aeroacoustic data, with simultaneous measurement of thrust and noise, have been generated with all possible combinations of baseline and modified nozzles. First, it is verified that all the primary beveled nozzles have the same mass flow as the baseline round over a range of nozzle pressure ratios; the flow path of the secondary nozzle is modified without altering the nozzle exit area. Therefore, all the nozzle combinations pass the same mass flow rates for fixed plenum conditions, and produce approximately the same absolute thrust. The experimental measurements confirm the expected trends of 1) deflection toward the short lip for the bevel, with progressively increasing deflection angle from ~ 1 deg for bevel 18 to ~ 2.2 deg for bevel 36; 2) deflection toward the long lip for the modified secondary, with MF2 producing a larger deflection; and 3) the combination of bevel + modified secondary counteracting the deflection due to the bevel alone and redirecting the jet plume toward the jet axis (and beyond), depending on the combination of the two nozzles. The thrust performance of a few of the nozzle combinations is within the error bar of the experimental measurements. In general, the largest bevel angle of 36 deg results in an unacceptably large thrust degradation and will not be suitable for practical application. It seems possible to design an acceptable nozzle system with a maximum bevel angle of ~ 30 deg and an appropriately designed modified secondary nozzle.

Under static conditions, both the modified secondary nozzles yield spectral reductions in the peak radiation sector in the aft quadrant. Thus, it is verified that the flow patterns created by the modified nozzles with a round primary, which mimic the flow cross sections of a beveled primary nozzle, can lead to noise reduction in the aft angles. Even with the introduction of forward flight stream, there is noise reduction for the modified secondary nozzles. Thus, one of the fundamental questions is answered: the modifications to the secondary nozzle as envisaged in this study are effective both at static and wind-on situations. In addition, the modified secondary nozzle provides the ability to deflect the plume away from the underside of the wing and the flap, thereby reducing the jet-flap interaction noise.

The cumulative noise benefit for the various nozzle geometries is established through the calculation of the effective perceived noise level (EPNL). An examination of the directivity of the perceived noise level indicates that there could be a small increase in level, relative to the baseline, of ~ 1 PNdB at the lower polar angles in the forward quadrant; however, this small increase is more than overcome by significant noise reduction of ~ 3 to ~ 4 PNdB in the peak noise radiation sector, typically for polar angles $\geq \sim 120$ deg. There is a net reduction in EPNL for all the nozzle geometries evaluated in this investigation. The combinations of modified secondary nozzles to bevel 24 and bevel 30 provide the largest reduction in EPNL over a wide range of freestream Mach number. The noise benefit at $\phi = 0$ deg varies from ~ 2.5 EPNdB at $M_t = 0.0$ to ~ 2.0 EPNdB at $M_t = 0.20$, to ~ 1.2 EPNdB at $M_t = 0.28$. These results, taken together with low thrust loss for these nozzle combinations, signify that the optimum bevel angle lies somewhere in this angular range from an aeroacoustic perspective. A point design for a modified secondary nozzle for a particular bevel angle in this desirable range is feasible with the design methodology developed and evaluated here. The synergistic melding of computational simulations with experimental measurements highlights the power of a joint approach and represents a significant step in nozzle design for noise reduction and low thrust penalty.

References

[1] Olsen, W. A., and Friedman, R., “Jet Noise from Coaxial Nozzles Over a Wide Range of Geometric and Flow Parameters,” AIAA Paper 74-43, 1974.

[2] Kozlowski, H., and Packman, A. B., “Aeroacoustic Tests of Duct-Burning Turbofan Exhaust Nozzles,” NASA CR-2628, 1976.

[3] Tanna, H. K., Tester, B. J., and Lau, J. C., “The Noise and Flow Characteristics of Inverted-Profile Coannular Jets,” NASA CR-158995, 1979.

[4] Goodykoontz, J. H., and Stone, J. R., “Experimental Study of Coaxial Nozzle Exhaust Noise,” AIAA Paper 79-0631, 1979.

[5] Tanna, H. K., “Coannular Jets—Are They Really Quiet and Why?” *Journal of Sound and Vibration*, Vol. 72, No. 1, 1980, pp. 97–118. doi:10.1016/0022-460X(80)90710-5

[6] Lu, H. Y., “Effect of Excitation on Coaxial Jet Noise,” *AIAA Journal*, Vol. 21, No. 2, 1983, pp. 214–220. doi:10.2514/3.8056

[7] von Glahn, U., and Goodykoontz, J. H., “Noise Suppression Due to Annulus Shaping of a Conventional Coaxial Nozzle,” NASA TM 81461, April 1980.

[8] Bhat, V. W., and Wright, C. P., U.S. Patent 4288984 for “Noise Suppressing Turbofan Nozzles and Method,” filed Sept. 1981.

[9] Seiner, J. M., and Krejsa, E. A., “Supersonic Jet Noise and the High Speed Civil Transport,” AIAA Paper 89-2358, July 1989.

[10] Papamoschou, D., “Fan Flow Deflection in Simulated Turbofan Exhaust,” *AIAA Journal*, Vol. 44, No. 12, 2006, pp. 3088–3097. doi:10.2514/1.22552

[11] Papamoschou, D., “Pylon-Based Jet Noise Suppressors,” *AIAA Journal*, Vol. 47, No. 6, 2009, pp. 1408–1420. doi:10.2514/1.37780

[12] Zaman, K. B. M. Q., and Papamoschou, D., “Effect of a Wedge on Coannular Jet Noise,” AIAA Paper 2006-7, Jan. 2006.

[13] Zaman, K. B. M. Q., Bridges, J. E., and Papamoschou, D., “Offset Stream Technology—Comparison of Results from UCI and GRC Experiments,” AIAA Paper 2007-438, Jan. 2007.

[14] Majjigi, R. K., Brausch, J. F., Janardan, B. A., Balsa, T. F., Knott, P. R., and Pickup, N., “Free Jet Feasibility Study of a Thermal Acoustic Shield Concept for AST/VCE Application,” NASA CR-3758, 1984.

[15] Bridges, J. E., and Henderson, B., “QAT Jet Noise,” *Technical Working Group Meeting*, NASA TM 2007-214992, June 2006.

[16] Brown, C., Bridges, J. E., and Henderson, B., “Offset Stream Technology Test—Summary of Results,” AIAA Paper 2007-3664, May 2007.

[17] Viswanathan, K., “Nozzle Shaping for Reduction of Jet Noise from Single Jets,” *AIAA Journal*, Vol. 43, No. 5, 2005, pp. 1008–1022. doi:10.2514/1.11331

[18] Viswanathan, K., “An Elegant Concept for Reduction of Jet Noise from Turbofan Engines,” *Journal of Aircraft*, Vol. 43, No. 3, May–June 2006, pp. 616–626. doi:10.2514/1.11432

[19] Viswanathan, K., “Noise of Dual-Stream Beveled Nozzles at Supercritical Pressure Ratios,” *Journal of Aircraft*, Vol. 43, No. 3, May–June 2006, pp. 627–638. doi:10.2514/1.11433

[20] Viswanathan, K., Shur, M., Spalart, P. R., and Strelets, M., “Flow and Noise Predictions for Single and Dual-Stream Beveled Nozzles,” *AIAA Journal*, Vol. 46, No. 3, March 2008, pp. 601–626. doi:10.2514/1.27299

[21] Shur, M. L., Spalart, P. S., and Strelets, M., “Noise Prediction for Increasingly Complex Jets. Part I: Methods and Tests,” *International Journal of Aeroacoustics*, Vol. 4, Nos. 3–4, 2005, pp. 213–246. doi:10.1260/1475472054771376

[22] Shur, M. L., Spalart, P. S., and Strelets, M., “Noise Prediction for Increasingly Complex Jets. Part II: Applications,” *International Journal of Aeroacoustics*, Vol. 4, Nos. 3–4, 2005, pp. 247–266. doi:10.1260/1475472054771385

[23] Shur, M. L., Spalart, P. S., Strelets, M., and Garbaruk, A. V., “Further Steps in LES-Based Noise Prediction for Complex Jets,” AIAA Paper 2006-485, Jan. 2006.

[24] Strelets, M. K., “Detached Eddy Simulation of Massively Separated Flows,” AIAA Paper 2001-0879, Jan. 2001.

[25] Ffowcs Williams, J. E., and Hawkings, D. L., "Sound Generation by Turbulence and Surfaces in Arbitrary Motion," *Philosophical Transactions for the Royal Society of London, Series A, Mathematical and Physical Sciences*, Vol. 264, No. 1151, 1969, pp. 321–342. doi:10.1098/rsta.1969.0031

[26] Gulyaev, A. N., Kozlov, V. E., and Secundov, A. N., "A Universal One-Equation Model for Turbulent Viscosity," *Fluid Dynamics*, Vol. 28, No. 4, 1991, pp. 484–494.

[27] Shur, M., Strelets, M., Zaikov, L., Gulyaev, A., Kozlov, V., and Secundov, A., "Comparative Numerical Testing of One- and Two-Equation Turbulence Models for Flows with Separation and Reattachment," AIAA Paper 1995-0863, Jan. 1995.

[28] Viswanathan, K., "Jet Aeroacoustic Testing: Issues and Implications," *AIAA Journal*, Vol. 41, No. 9, 2003, pp. 1674–1689. doi:10.2514/2.7313

[29] Viswanathan, K., "Instrumentation Considerations for Accurate Jet Noise Measurements," *AIAA Journal*, Vol. 44, No. 6, 2006, pp. 1137–1149. doi:10.2514/1.13518

[30] Shields, F. D., and Bass, H. E., "Atmospheric Absorption of High Frequency Noise and Application to Fractional-Octave Band," NASA CR 2760, 1977.

[31] Amiet, R. K., "Correction of Open Jet Wind Tunnel Measurements for Shear Layer Refraction," AIAA Paper 75-532, 1975.

[32] Amiet, R. K., "Refraction of Sound by a Shear Layer," *Journal of Sound and Vibration*, Vol. 58, No. 4, 1978, pp. 467–482. doi:10.1016/0022-460X(78)90353-X

[33] Viswanathan, K., "Distributions of Noise Sources in Heated and Cold Jets: Are They Different?" *International Journal of Aeroacoustics*, Vol. 9, Nos. 4–5, 2010, pp. 589–626. doi:10.1260/1475-472X.9.4-5.589

[34] Viswanathan, K., "True Farfield for Dual-Stream Jet Noise Measurements," *AIAA Journal*, Vol. 49, No. 2, 2011, pp. 443–447. doi:10.2514/1.J050771

A. Lyrintzis
Associate Editor